Research Square

Preprints are preliminary reports that have not undergone peer review.
They should not be considered conclusive, used to inform clinical practice,
or referenced by the media as validated information.

The Influence of Physiological Oxygen Levels on the Composition and Phenotype of Tenocyte-Derived Extracellular Vesicles

Amy Byrne

amy.byrne@nihr.ac.uk

NIHR https://orcid.org/0009-0002-1418-7454

Nicholas Wrag

Keele University

Marta Clerici

University of Salerno

Nicholas Forsyth

Keele University

Research Article

Keywords: Tendon, Extracellular vesicles, secretome, conditioned media, hypoxia, immune modulation

Posted Date: April 29th, 2026

DOI: https://doi.org/10.21203/rs.3.rs-9370200/v1

License: This work is licensed under a Creative Commons Attribution 4.0 International License.
Read Full License

Additional Declarations:
The authors declare no competing interests.

Experiments were performed in accordance with the EU guidelines for using food chain animal tissues & human cell lines for research purposes and the guidelines of the UK Human Tissue Act (Scientific Procedures) Act 1986 and its subsequent amendments. Use of animal products and human cell lines in this project was approved by the Animal Welfare and Ethical Review Body for the University of Keele and carried out under the terms of UK Home Office Licenses PP4353554, P9B1FBC4B and 70/7715, and the Ethical Review Body by the UK human tissue act.

(Byrne et al., 2013) *(Article.)*

Tenocyte-derived extracellular vesicles and secretome have distinct compositions.

Amy L Byrne1, Dr N.Wragg1, and Nicholas R Forsyth1, 2, *

1School of Pharmacy and Bioengineering, Keele University, Stoke-on-Trent, Staffordshire ST4 7QB, UK.

2 Vice Principals' Office, University of Aberdeen, Kings College, Aberdeen, AB24 3FX, UK.

*Correspondence: nicholas.forsyth@abdn.ac.uk

Abstract: Tendinopathy is a multifactorial spectrum of disorders, characterized by tendon pain that often worsens with activity. These disorders account for a high proportion of clinical referrals and consequently have a large socioeconomic disease burden. Currently we have an incomplete understanding of the pathophysiology of tendon diseases which hampers the development of adequate treatments. We hypothesized that the tenocyte may play a role in immediate disease or damage resolution via release of its secretome or discrete extracellular vesicle (EV) populations. We therefore sought to isolate and characterize the tenocyte secretome and EVs to evaluate component characteristics and determine their potential for participation in tendinopathy resolution. Isolating small extracellular vesicles is key to understanding their mechanisms of action and how they can be used therapeutically. This work provides the first documented isolation and characteristion of tenocyte EV subpopulations, which have been subject to differing oxygen levels during culture and demonstrates that oxygen levels during TNC EV harvesting significantly influences the resulting EV populations and plays an important role in determining their surface markers and associated cytokine profiles.

Tenocytes cultured in physiological oxygen levels have an increased population doubling potential and increased levels of CD73 expression when compared to tenocytes cultured in air oxygen / hyperoxia. Tenoctye EV subgroups differed between conditions with physoxia resulting in significantly higher numbers of EVs with diameters of <250nm when compared to air oxygen. EV protein and lipid concentrations were also significantly influenced by oxygen concentration with air oxygen EV samples containing significantly less protein in CM, crude EVs, and small EVs. Surface marker characterization demonstrated that all EV subgroups displayed tetraspanin; CD8, CD69, and CD81. Increased tetraspanin expression, specifically CD8 and CD69, was observed for EV subgroups in physoxia as were stem cell associated markers (SSEA-4, CD105, CD90, CD73 and ROR1). Air oxygen EVs displayed increased CD20 and CD45 expression vs. physoxia. Cytokine analysis of the tenocyte secretome; CM and EV subgroups in physoxia demonstrated increased levels of anti-inflammatory cytokines in CM and EV subgroups, specifically IL-10, IL-2 and IL-4. Air oxygen conditions produced significantly higher levels of inflammatory cytokines across the EV subgroups; GMCSF, IL6, IL8, TNF-α, and IL-18. These findings demonstrate the importance of physoxia for EV production and the potential of using oxygen levels as a tool to yield specific EV phenotypes.

Tenocyte derived EVs have largely been unexplored due to the promise of stem cell derived EVs but these findings demonstrate that tenocyte EV subgroups display specific phenotypes in response to oxygen levels during culture. This work provides fundamental information to proceed to determining the clinical utility of tenocyte EVs, further research using robust isolation and characteristics needed to fully understand the potential of TNC EVs.

Keywords: 1; Tendon 2; Extracellular vesicles. 3; secretome. 4; conditioned media. 5; hypoxia. 6; immune modulation.

1.Introduction

1.1. The tendon injury and clinical profile

Tendinopathy is an overuse injury accompanied by high rates of disability and is amongst the most common complaints in patients seeking medical attention (Pabón & Naqvi, 2021). It is estimated to occur in up to 25% of reports from occupational settings and in up to 50% of athlete injuries (Lancaster & Mahadevan, 2021). Major tendons experience high loads and dynamic forces, the Achilles tendon, in example, routinely experiences up to 12.5 times the weight of an individual. Repetitive strain and overload trigger the accumulation of microtears and dysregulated inflammatory and degenerative processes (Khan et al., 1999). Overt symptoms are secondary to inflammatory cellular process and tendinous matrix remodeling, where symptoms include swelling, pain, and functional limitations (Abate et al., 2009). Tendons have a low metabolic rate and limited vascularity requiring long periods of rest to achieve only suboptimal fibrovascular tissue repair, which is prone to rupture. Annually tendinopathy has an estimated associated expense of $30 billion, which is a driving force behind research efforts into understanding the molecular basis of tendinopathy (Maffulli et al., 2020).

In this context, the specific molecular processes that orchestrate immunomodulation in tendinopathy, and how we can harness this ability to trigger regeneration, establish prominence. These are required due to their being no therapies established to regenerate tendon fully Tendon injury triggers an inflammatory response that is defined by the expression of pro inflammatory mediators, immune cell infiltration, and a subsequent decrease in collagen synthesis (Tsuzaki et al., 2003). Matrix metalloproteinase (MMPs) expression is triggered along with angiogenesis and vasodilation (Chisari et al., 2020). The metabolic activity of tendon is increased, and the phenotype shifts to a pro-inflammatory phenotype and with production of cytokines; TNF-α, IL-1β, IL-6, IL-10, VEGF and TGF-β, sustained inflammatory responses drive tendinopathy (Jones et al., 2013). Often tendinopathies originate when this inflammatory response is not fully resolved, leading to a dysregulation within the extracellular matrix (ECM) remodeling process (Millar et al., 2017). This dysfunction causes a decrease in the amount of collagen produced and its anisotropic organization is disrupted, resulting in weaker and less flexible tendons, more likely to rupture. Current medical therapies to manage symptoms include managing pain, steroidal anti-inflammatories, rest and physiotherapy over at least 3 months, which has a low rate of compliance. When rest and physiotherapy are not adequate in providing relief, surgery is sometimes indicated (Huttunen et al., 2014). However, none of these treatments can fully restore tendon structure and function. Treatments often result in gradual degeneration and rupture. The production of new, effective treatments is vital and a focus on modulating the inflammatory response and resolving ECM dysregulation to allow for tendon regeneration could provide this (Russo et al., 2022).

1.2. The tendon secretome and its associated extra cellular vesicles

Proteins secreted from cells are often exploited as targets and are collectively referred to as the secretome (Mitchell et al., 2019). Characterization of the secretome can provide essential information in defining a cell's response to its microenvironment in health and disease. This information can potentially be used to develop therapeutics and biomarkers. Extracellular vesicles (EVs) are a secretome component and are membrane bound vesicles with the ability to transport and deliver a wide array of cargo including, proteins (associated with the cell of origin plasma membrane), micro-RNA (miRNA), and lipids (Doyle & Wang, 2019) (Gurung et al., 2021). They are responsible for the regulation of biological functions, including immune regulation, angiogenesis, ECM remodeling, and stem cell differentiation. EVs are classified according to their size, density, and biogenesis where small EVs, formerly called exosomes, range from 30-500 nm and medium extra cellular vesicles; 500-1500 nm (Al Halawani et al., 2022; Gurung et al., 2021). The interest in EVs for application as biomarkers and treatments have grown over the last 2 decades (Al Halawani et al., 2022), with promising results in clinical trials and in vitro studies across a wide range of indications (Y. Wang et al., 2019a). EVs have lower immunogenicity than cell-based therapies and greater stability than cytokines alone, due to their lipid encapsulation (Doyle & Wang, 2019). The EV field of research is largely based on stem and immune cell derived EVs. Tendon specific EVs are largely unexplored with little data on their utility or characterization (Y. Wang et al., 2019b). EV isolation and characterization are often problematic, with poor reproducibility, inefficient isolation, incomplete characterization, definitions of vesicle subtypes, and crossover within these categories create challenges in interpretation(Van Deun et al., 2014).

1.3. Models in tendon research

Animal models provide a vital cornerstone for translational medical research including exploration of basic pathophysiology when challenges in sourcing clinical or waste materials exist. However, circa

90% of approaches fail to translate basic science to clinical treatment, often due to inefficiencies, safety, and cost (Oreffo et al., 2021). These failures cost animal lives and burden biomedical research. Common problems with animal model utility in tendon research, specifically tendinopathy, emerge due to the lack of in-depth validation studies of animal models beyond structural repair. The specific biochemical and mechanical similarities of animal models are lacking. Human tendons are often obtained from individuals of advanced age and/or with underlying pathologies while animal model systems allow the ready isolation of healthy, primary, tenocytes. There are many studies examining and validating the utility of various animal models including rat, mice, sheep, horse, rabbits and pigs (Domnick et al., 2016). Porcine tendons have repeatedly demonstrated that they share physical and chemical characteristics with human tendons (M Bottagisio, 2017).

However, no individual species has established itself as the gold standard for fundamental tendon research. Porcine tenocytes share common characteristics with human tenocytes, both have a fusiform appearance and display similar dimensions in length and width. Further, at high confluency porcine and human tenocytes both create bundles arranged in a storiform patterns (Lui et al., 2011). Decellularized porcine flexor and extensor tendons act as surrogates for human tendons in biomechanical studies and are used clinically as grafts for anterior cruciate ligament (ACL) reconstruction, evidencing their compatibility with human biology (Loh et al., 2018). GM-CSF is found in high levels in joints with tendiopathy and blocking GM-CSF as a biological target for new theraputics as a way to modulate inflammation and improve repair for example otilimab was developed to block GM-CSF(C. Buckley et al., 2020; C. D. Buckley et al., 2020; Bykerk, 2020; Genovese et al., 2020).IL-6 is often present in higher amounts during initial acute stages of damage and is also involved in human tendon disease its presence outside of the acute phase its presence is linked tendon rupture/tears, whereas IL-1β, IL-6, and TNF-α tended to be increased in animal models of tendon injury, the roles of IL-1β, IL-6, IL-10, and TNF-α in the development of tendon disease, during tendon healing, and in response to exercise. However, there is evidence accumulating that suggests that other cytokines are also contributing to tendon inflammatory processes.

2.0. Results

2.1. Isolation and Characterization of Primary Tenocytes

Following explant of porcine dorsal flexor tendon (Figure 1A), we observed migration of spindle or polygonal shaped cells from tissue within 3–5 days in physoxia and 5-7 days in air oxygen (Figure 1B). Recovered cells displayed positive tenomodulin expression in both air oxygen and physoxia, with no difference observed in intensities (Figure 1C, physoxia shown). Cumulative population doubling (CPD) indicated that tenocytes displayed an elevated proliferative potential in physoxia (CPD 40) compared to air oxygen (CPD 31). This was evident from day 3 and a increased proliferation rate was sustained until the experiment end point (day 60) for tenocytes cultured in physoxia. (Figure 1D).

Mesenchymal stromal cells (MSCs) were used as a positive control for tenocyte stem cell marker expression. MSCs isolated from a commercially sourced donor bone marrow aspirate were cryopreserved at P2 then thawed for subsequent analysis(Bullough et al., 2008; Kay et al., 2017). As anticipated MSCs expressed the surface markers CD73, CD90, and CD105 (>95% positive) while being negative for CD14, CD19, CD34, and CD45 (<5% positive). No significant differences were noted between physoxia and air oxygen expression levels (Figure 1E). Tenocytes lacked CD90 expression (<5%) but were positive for both CD73 and CD105. We noted that unlike MSCs, tenocytes displayed significantly elevated CD73 in air oxygen (32%) vs. physoxia (13%) while the converse was true with CD105, physoxia 41% and air oxygen 32% ($p<0.05$). Irrespective of the changes noted the overall expression levels of CD73, CD90, and CD105 were markedly lower in tenocytes vs. MSCs. Tenocytes and MSCs both lacked expression of hematopoietic stem cell markers, including CD14, CD19, CD34, or CD45, irrespective of culture conditions (<5%) (Figure 1E). Finally, we sought to determine whether tenocytes displayed a classical trilineage differentiation potential (Figure 1F). Histological evaluation confirmed that tenocytes underwent bone (Alizarin red), cartilage (Alcian blue), and fat (Oil red O) differentiation.

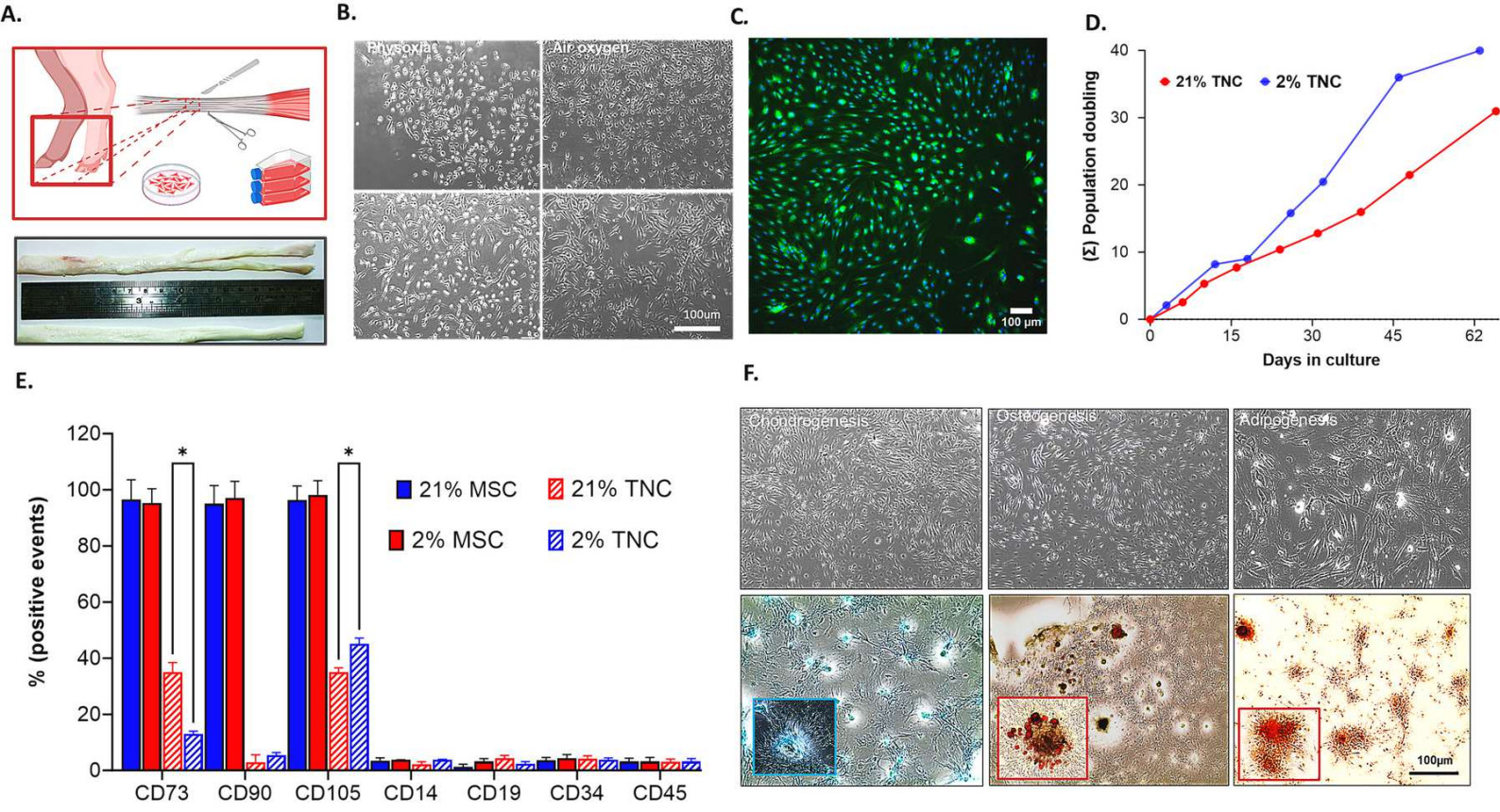


Figure . ***Porcine tenocytes express selected stem cell markers and undergo multilineage differentiation.*** ***A.*** *(Upper) Schematic indicating tenocyte explant protocol. Tenocytes were obtained from three biologically separate porcine dorsal flexor tendons (lower) that were isolated, minced, and explanted.* ***B.*** *Tenocytes at passage 0 and 7 in air oxygen and physoxia.* ***C.*** *Representative image of tenomodulin (green) immunostaining of passage 2 tenocytes (physoxia), DAPI (blue) nuclear counterstaining. Scale bar: 100 µm.* ***D.*** *Tenocyte cumulative population doublings in physoxia and air oxygen over a 60-day period.* ***E.*** *Tenocyte stem cell marker expression in comparison to bone marrow derived MSCs (n=3 biological replicates, mean ± SD, * indicates p<0.05).* ***F.*** *Trilineage differentiation of cultured tenocytes at physiological oxygen; upper: tenocytes with growth medium (Bottom), lower: tenocytes in lineage specific differentiation medium (Top) scale bar: 100 µm*

2.2. Tenocyte secretome and Extracellular vesicle subpopulations

Following on from tenocyte isolation and characteristion we sought to determine secretome characteristics through investigation of tenocyte conditioned media (TNC CM) and following its ultracentrifugation and density gradient centrifugation its isolated, crude EVs (C.EVs), and small EVs (S.EVs), respectively. Analysis of air derived S.EVs demonstrated a relative, average frequency of 80 particles with a diameter of <250 nm. In comparisson physoxia cultured tenocytes produce significantly more particles with a diameter of less than 250 nm, with an relative average number of 130 ($p<0.05$) (Figure 2A). Representative scanning electron microscopy (SEM) images, that were used for the analysis described above of C.EVs and S.EVs both displayed homogenous populations, with a wide variety of sizes and morphologies observed (Figure 2B). Particle size measurement indicated that vesicle subpopulations displayed significantly different diameters indicating the efficacy of the density gradient to separate/purify EV preparations. Following the same pattern as the image analysis, size measurements also displayed oxygen-dependent differences in the averages sizes of EVs (Figure 2C). TNC CM at physyoxia displayed a 1.19-fold increase in particle size when compared to crude Evs obtained in air oxygen culture with a mean particle diameter of 5100 nm for physoxia vs. 4200nm air oxygen, $p<0.005$. TNC crude EV subpopulations had an average particle diameter of 690 nm for air and 550 nm physoxia $P<0.01$. Small EVs displayed a radius of 125 nm for air oxygen and a significantly smaller 87 nm in physoxia ($p<0.05$). Taken together this highlights a role for physoxia culture of tenocytes to influence size determination (Figure 2C).

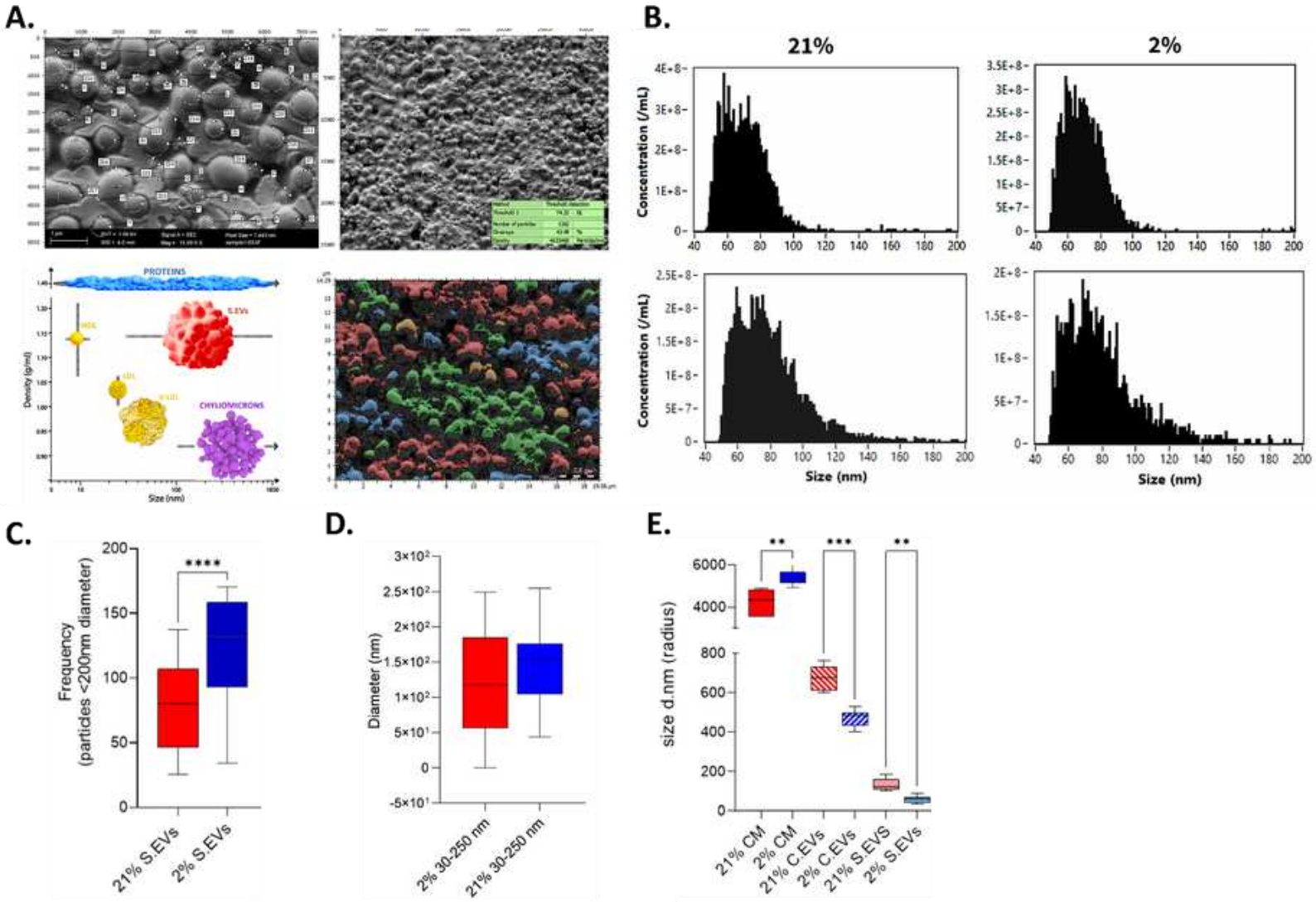


Figure 2: Tenocyte secretome particle diameters reduce with increasing purity. *A. Representative SEM Images of TNC EV with corresponding measurements, parameters used for counts and masking.(right) lower magnification image with detection setings for Mountains SEM softwear (scale 1µm. Images obtained for all biological replicates in air and physoxia for all subgroups. Bottom left displays an briefe overview of the secretome contents and their size overlaps. B. Histogram representing submicron particle detection by nano FCM. Size profiles, mean particle size (nm) and particle concentration (particles/mL) of isolated TNC EV subgroups at air and physoxia were acquired by nano-flow cytometry. TNC S.EVS in air oxygen are larger and more heterogeneous than S.EVs collected at (x axis size nm, y particle number per ml, p<0.05.C. Frequency of Particle diameter measurements of S.EVs in air and physoxia for three independent biological replicates. Data show represents mean and standard deviation of these replicates. D. Particle diameters of TNC EV subroups in air and physoxia. y axis = particle radius. Data shown as mean and standard deviation for three biological replicates*p<0.05.E Dynamic light scattering diameter measurements for all subroups at air and physoxia, y-axis-diameter (nm) n=3*, **0.002, ***0.001 *****0.0001*

2.3. Protein and lipid levels of Tenocyte EVs are influenced by oxygen levels during culture.

Extracellular vesicle (EV) protein levels are significantly influenced by oxygen concentration during tenocyte culture. Specifically, tenocytes cultured under **physiological oxygen (physoxia)** conditions tend to produce EVs with **higher protein content** compared to those cultured in air oxygen (hyperoxia). This trend is observed across different EV subpopulations, including conditioned media (CM), crude EVs (C.EVs), and small EVs (S.EVs).

2.3.1. Protein and lipid ratio.

Having confirmed particles in density centrifugation samples that matched an anticipated size profile of EVs we next sought to characterise their protein content. Protein conncentration was monitored for

all subgroups in both air and physoxia, a progressive decrease in protein and an increase in lipid content throughout the isolation is associated with the presence of EVs(Brennan et al., 2020). The protein content of increasingly fractionated samples followed an inverse trend to lipid content, where TNC CM > C.EVs > S.EVs (Figure 3A). As with lipid content and in agreement with previous data, physoxia consistently resulted in significantly higher protein content than air oxygen cultures. Specifically, air oxygen TNC CM samples contained an average of 655 µg/ml, whereas physoxia TNC CM contained 788µg/ml. TNC C.EVs in air oxygen (325 µg/ml) also contained less protein than TNC C.EVs from physoxia culture (588 µg/ml, $p<0.01$). Consistent with above we observed that air oxygen-derived S.EVs (15 µg/ml) displayed a decrease in protein yield relative to physoxia (31µg/ml) TNC S.EVs*** $P<0.001$ (Figure 3A).

2.3.2. Lipd content of TNC EVs

Total lipid concentration was determined for all EV subgroups in air and physoxia (Figure 3B). TNC CM contained the lowest levels of total lipid in air oxygen (35 ng/ml) and physoxia (49 ng/ml), albeit at higher levels in physoxia. Crude EV lipid content increased 10 Fold relative to CM samples. TNC CM lipid content was 0.2ug/ml for air and 0.51 ug/ml physoxia crude EVs at air contained 15ug/ml and and 21ug/ml for physoxia A significant lipid content was maintained in physoxia samples (0.51 ug/ml) compared to air oxygen (0.11ug/ml), ($p<0.05$). S.EV subpopulations displayed a further 3 fold increase of lipid content and, in agreement with CM and C.EVs, significantly higher amounts were detected in physoxia (33.9 ug/ml) compared to air oxygen (29.1 ug/ml), ($p<0.01$). Increasing purification of secretome components from CM to S.EVs was associated with reduced overall protein concentrations and an increased lipid to protein ratio (Figure 3C). **Conditioned Media (CM):** Tenocyte CM from physoxia cultures shows **higher protein content** compared to CM from air oxygen cultures. Air oxygen TNC CM samples contained an average of 655 µg/ml, whereas physoxia TNC CM contained 788 µg/ml. **Crude EVs (C.EVs):** C.EVs isolated from physoxia cultures have significantly **higher protein levels** compared to C.EVs from air oxygen cultures. TNC C.EVs in air oxygen (325 µg/ml) contained less protein than TNC C.EVs from physoxia culture (588 µg/ml, $p<0.01$).**Small EVs (S.EVs):** S.EVs from physoxia cultures exhibit significantly **higher protein content** than those from air oxygen cultures. Air oxygen-derived S.EVs (15 µg/ml) displayed a decrease in protein yield relative to physoxia (31µg/ml) TNC S.EVs*** $P<0.001$. The increased protein levels observed in EVs from physoxia cultures may have implications for EV function, including their interaction with target cells and cargo delivery. Further research is needed to understand how the specific protein cargo of EVs is affected by oxygen levels and how this may impact their therapeutic potential.

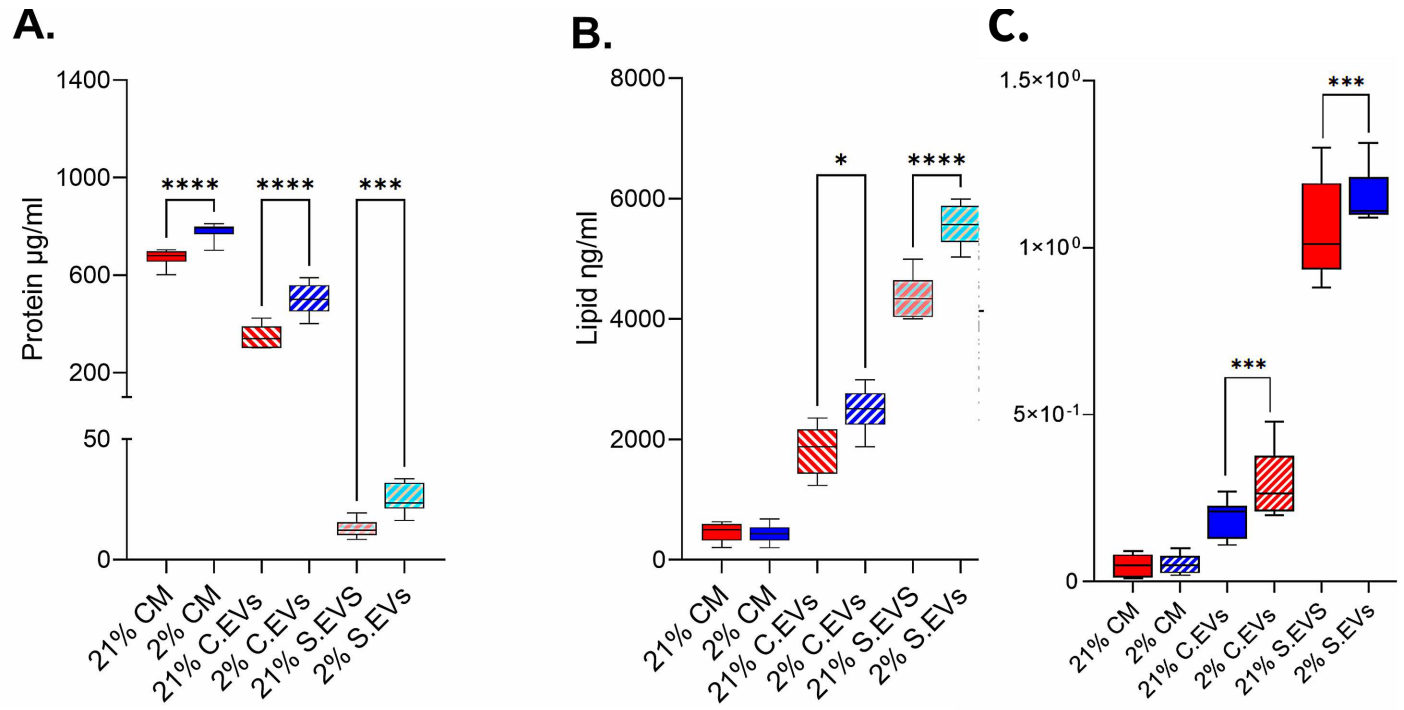


*Figure 3. **Isolation of EV fractions from CM results an increased lipid to protein sample content. A**. Total protein content for CM, crude EVs, and small EVs from air oxygen and physoxia cultured TNC secretome subgroups. B. Lipid content determined by Sulfo-Vanillin assay for the tenocyte secretome subgroups; CM,N C.EVs and S EVs in air and physoxia. **C.** Protein-to-lipid ratios were calculated for C.EVse and S. EVs for air and physoxia samples for all biological replicates. Mean ± SD, n=3 biological replicates, *p<0.05, **p<0.01, ***p<0.001, ****p<0.0001.*

2.4 Vesicle size, concentration and EV RNA staining by Nano- flow cytometry characterisation.

TNC EV subpopulations were stained with SYTO green to identify extra cellular vesicles carrying nucleic acid (RNA) while concentration and size were obtained by nanoFCM analysis of all TNC EV subgroups. Ultra centrifugation alone (used to obtain C.EVs) resulted in less EVs positively stained for RNA, along with lower particle concentration and larger size than EV samples obtained via density gradient ultra centrifugation (S.EVs) (Figure 4 A, B). This indicated that density gradient ultracentrifugation was effective for isolating small and homogeneous (20-500nm) populations of vesicles, particle concentration and size of S.EVs at air is shown in figure 4A and for air and physoxia S.EVs in figure , nano-FCM was used to obtain size and concentration. Sytox green RNA stain was used to stain S.EV samples to identify RNA present on either the EV surface or free within the sample solution via nano-flow cytometry, positive and negative events detected via FITC are shown in figure 4C. levels of positive events for S.EVs at air and physoxia were not significantly different.

2.5. TNC EV surface marker expression characterisation.

Overall, increased fractionation to small EVs increased the detectable levels of the majority of EV surface markers in both physoxia and air oxygen samples (Figure 4A).The heat map (Figure 4D) demonstrates changes in marker expression within each subgroup in air and physoxia (Figures 5, 6, & 7 provide detailed breakdown and expression levels). Broadly speaking expression levels of all markers were substantially elevated in S.EVs vs. C.EVs irrespective of oxygen culture condition applied. Immune-Associated Markers: Air oxygen EVs display increased expression of CD20 and CD45 compared to physoxia EVs. S.EVs show increased expression of CD146, CD209 and HLA-1 in physoxia.CD56 is upregulated in air oxygen S.EVs, while other immune-associated markers are generally upregulated in physoxia S.EVs.

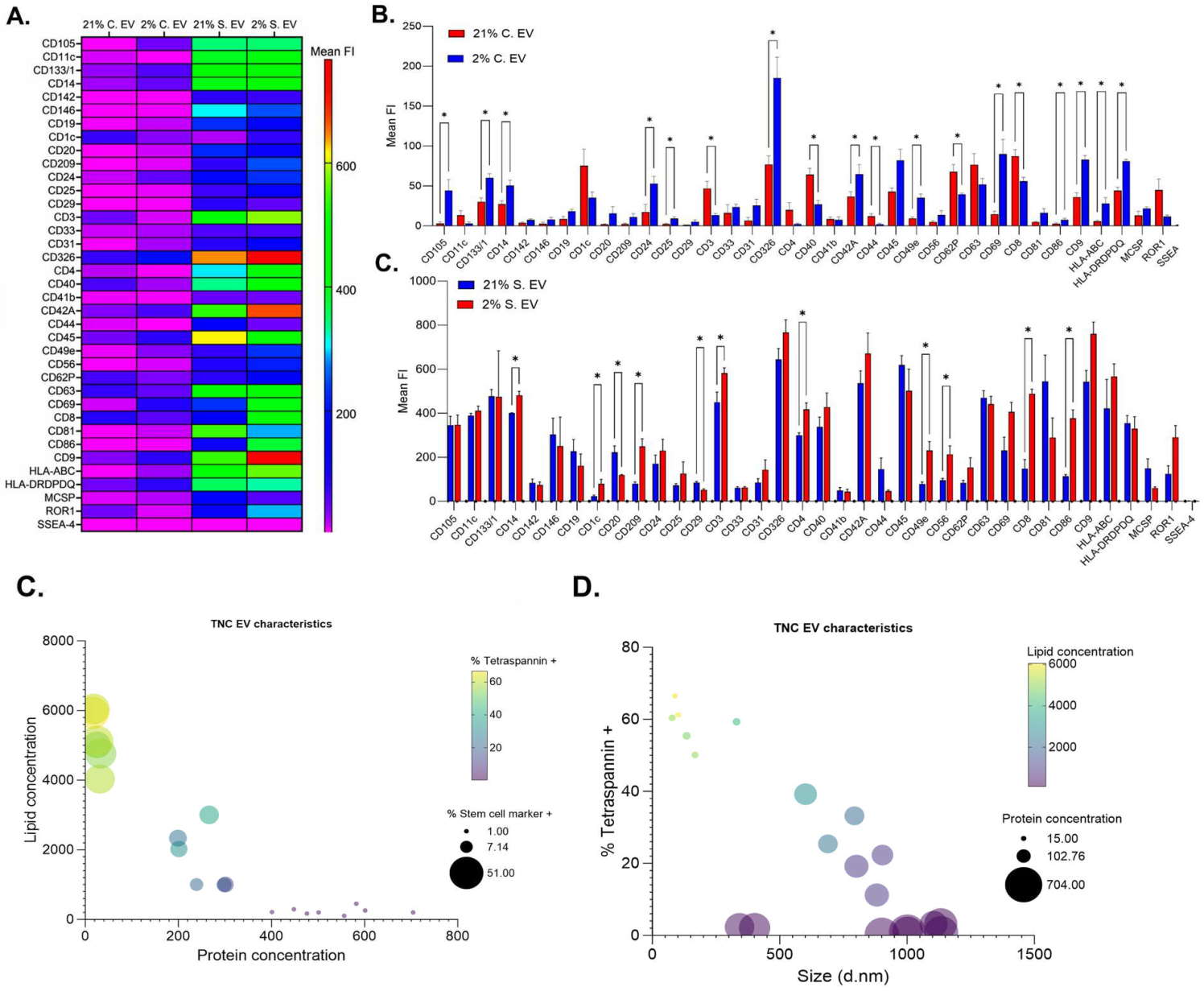


Figure 4. Characterization of Tenocyte Extracellular Vesicle (EV) Surface Markers and Physicochemical Properties.(A) Heatmap of EV Surface Marker Expression: This heatmap displays the mean fluorescence intensity (MFI) of various surface markers (CD antigens, HLA, etc.) on EVs isolated from tenocytes cultured under 21% O2 (normoxia) and 2% O2 (physoxia). The color scale on the right indicates the MFI range, with warmer colors (red, yellow) representing higher expression and cooler colors (blue, green) representing lower expression. This provides a comprehensive overview of the immunophenotype of the EV populations under different oxygen conditions. (B) Comparison of Surface Marker Expression on Crude EVs (C.EVs): This bar graph presents the mean fluorescence intensity (MFI) of specific surface markers on Crude EVs (C.EVs) derived from tenocytes cultured at 21% O2 (white bars) versus 2% O2 (red bars). Error bars represent standard error of the mean (SEM). Asterisks (*) indicate statistically significant differences between the two oxygen conditions ($p < 0.05$). This panel highlights specific changes in surface protein expression on C.EVs in response to varying oxygen levels.(C) Comparison of Surface Marker Expression on Small EVs (S.EVs): Similar to panel B, this bar graph shows the mean fluorescence intensity (MFI) of surface markers on Small EVs (S.EVs) derived from tenocytes cultured at 21% O2 (white bars) versus 2% O2 (red bars). Error bars represent SEM, and asterisks (*) denote statistically significant differences ($p < 0.05$). This panel focuses on the immunophenotypic differences observed specifically within the S.EV subpopulation.(D) TNC EV Characteristics: Lipid Concentration vs. Protein Concentration: This scatter plot visualizes the relationship between lipid concentration (y-axis) and protein concentration (x-axis) for Tenocyte EVs (TNC EVs). The size of each bubble represents the percentage of "stem cell markers" (e.g., specific CD markers associated with stemness), and the color gradient indicates the percentage of "Tetraspanin+" EVs (e.g., CD9, CD63, CD81), providing insights into the biochemical composition and subpopulation distribution of the EVs.(E) TNC EV Characteristics: % Tetraspanin+ vs. Size: This scatter plot explores the relationship between the percentage of "Tetraspanin+" EVs (y-axis) and EV size in nanometers (x-axis) for TNC EVs. The size of each bubble represents the protein concentration, and the color gradient indicates the lipid concentration. This panel helps to correlate the size, tetraspanin expression, and overall biochemical content of the isolated EV populations.

2.6. TNC EVs; tetraspannin expression.

The presence of tetraspanin markers CD8, CD9, and CD63, is a minimal requirement for identifying small EVs/exosomes, as defined by the International Society of Extracellular Vesicles, irrespective of culture condition. (ISEV MEVR, Royo et al., 2020). Small EVs (S.EVs) from physoxia cultures display increased expression of CD9 and CD69 when compared to S.EVs from air oxygen cultures. CD81 expression is greatly elevated in S.EVs, irrespective of culture conditions. S.EVs displayed robust CD9 expression significantly elevated in physoxia (86 MFI vs. 53 MFI in air oxygen). CD69 expression followed broadly the same pattern as CD9 displaying little expression in C.EVs from air oxygen (29 MFI) and slightly increased expression in those derived in physoxia (65 MFI). The overall expression profile of CD69 in S.EVs demonstrated a marked increase in physoxia (588 MFI) vs air (350 MFI) ($p<0.05$). CD81 displayed negligible expression in C.EVs in air (31 MFI) and physoxia (35 MFI) and greatly elevated expression in S.EVs, irrespective of culture condition, in air (504 MI) and physoxia (544 MFI) (Figure 5A).

2.7.TNC EVs; ROR1, SSE-4, CD133 and MCSP.

Both C.EVs and S.EVs under physoxia show increased expression of the following markers: SSEA-4, CD105, CD90, CD73 and ROR1. CD133/1 and significantly upregulated in S.EVs from physoxia compared to air oxygen. ROR1, MCSP, and SSEA4 all display little to no expression in S.EVs. TNC C.EVs displayed low levels of expression of ROR1 in physoxia (88 MFI) that were slightly upregulated in air (113 MFI), CD133/1 was upregulated in physoxia (204 MFI) vs. air (55 MFI), while MCSP displayed low levels of expression consistent across both conditions vs physoxia (15 MFI). S.EVs a significant increase was noted for CD133/1 in physoxia vs. air (601 vs. 235 MFI, $p<0.05$) while ROR1, MCSP, and SSEA4 all displayed little to no expression (all values <20 MFI). SSEA4 displayed negligible expression in all C.EVs (Figure 5B) S.EVs a significantly elevated expression was noted for CD133/1 in physoxia vs. air oxygen (601 vs. 235 MFI, $p<0.05$) TNC C.EVs displayed low levels of expression of ROR1 in physoxia (88 MFI) and slightly upregulated in air (113 MFI), CD133/1 was upregulated in physoxia (204 MFI) vs. air (55 MFI) (*$P<0.05$), while MCSP displayed low levels of expression consistent across both conditions air (11 MFI) vs physoxia (15MF), and while ROR1, MCSP, and SSEA4 all displayed little to no expression (all values <20 MFI) (Figure 6B).

2.8. TNC EV Integrin associated EV markers (CD11c, CD41b, CD42A, CD49e)

Integrin associated EV markers (CD11c, CD41b, CD42A, CD49e) followed broadly the same pattern as tetraspanins CD9 and CD69 with little to no expression in C.EVs and marked increases in S.EVs. Non-significant increases were observed for; CD49e, air (188 MFI) vs physoxia (381 MFI); CD42A, air (552 MF) vs physoxia (709 MFI); CD11c, air (377 MFI) vs physoxia (774 MFI). Significant increases in physioxia for C.EVs were observed for CD42A; air (31 MFI) vs physoxia (55 MFI) $p<0.05$. Figure 5C).

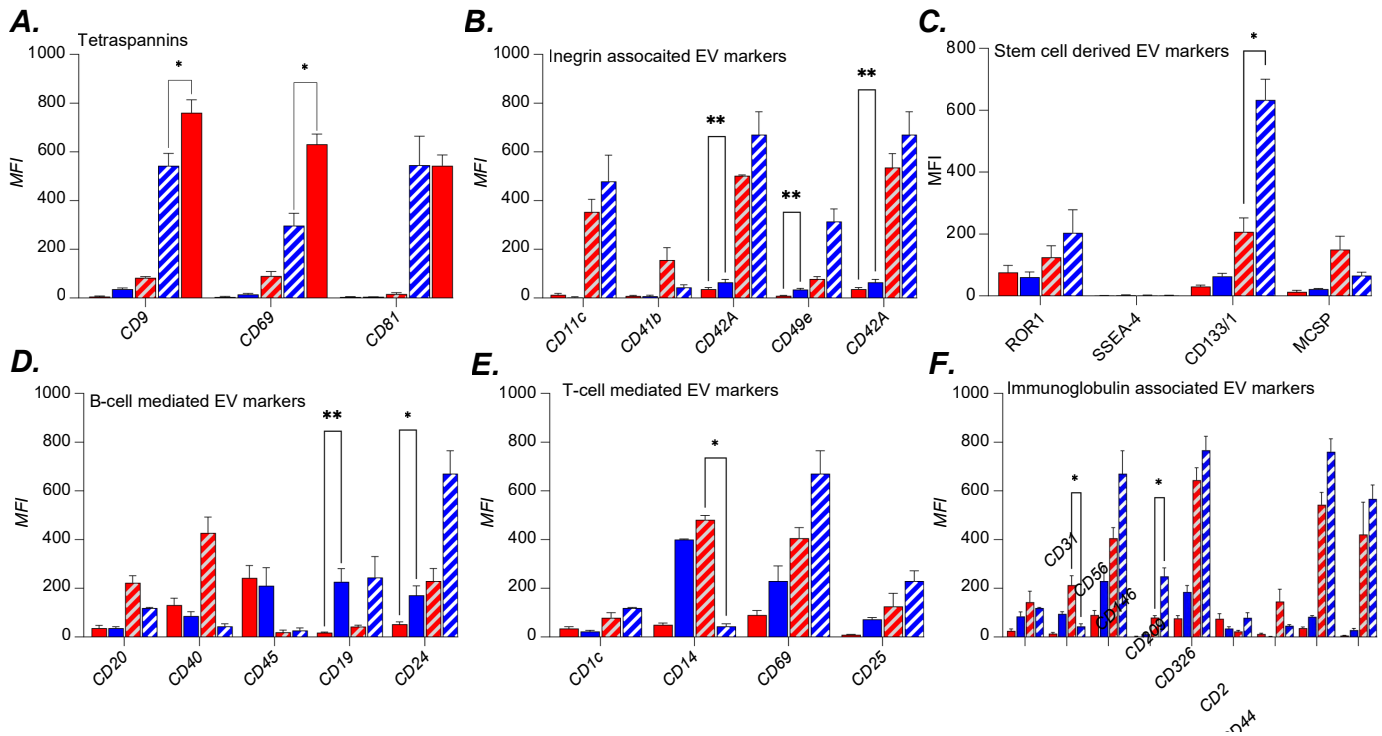


Figure 5 . Characterization of Extracellular Vesicle (EV) Surface Markers by Flow Cytometry. This figure presents the mean fluorescence intensity (MFI) of various surface markers on extracellular vesicles (EVs) isolated under different oxygen conditions (air vs. physoxia). Data are presented as mean ± standard error of the mean (SEM). Statistical significance was determined using [Insert Statistical Test Here, e.g., two-way ANOVA followed by post-hoc Tukey's test]. An asterisk (*) indicates a statistically significant difference ($p < 0.05$) between air and physoxia conditions for a given marker.A. Tetraspanin Markers: MFI of tetraspanin proteins (CD9, CD63, and CD81) on EVs derived from tenocyte conditioned media (TNC CM). Red bars represent EVs from air oxygen cultures, and blue bars represent EVs from physoxia cultures.B. Stem Cell Derived EV Markers: MFI of markers associated with stem cell-derived EVs (ROR1, SSEA-4, CD133/1, and MCSP). Red bars represent EVs from air oxygen cultures, and blue bars represent EVs from physoxia cultures. C. Integrin Associated EV Markers: MFI of integrin-associated EV markers (CD11c, CD41a, CD49a, and CD49e). Red bars represent EVs from air oxygen cultures, and blue bars represent EVs from physoxia cultures.. (D) B-cell mediated EV marker expression: CD20, CD40, CD45, CD19, and CD24. (E) Profile of T-cell mediated EV markers: CD1c, CD14, CD69, and CD25. (F) Characterization of immunoglobulin-associated markers and additional surface proteins, including CD31, CD56, CD146, CD209, CD326, CD2, CD44, HLA-1, and HLA-2.The y-axis represents the Mean Fluorescence Intensity (MFI). Data are presented as mean ± SD. Statistical significance is indicated by asterisks ($p < 0.05$, ** $p < 0.01$). Different experimental conditions are distinguished by solid and striped bar patterns.*

2.9 TNC C.EV Immune-associated markers;

Tenocyte extracellular vesicle (EV) surface marker expression is significantly influenced by oxygen levels during cell culture, with physoxia (physiological oxygen levels) generally promoting the expression of stem cell-associated markers and tetraspanins, while air oxygen (hyperoxia) leads to increased expression of certain immune-related markers. C.EV immunoglobulin markers at air and physoxia are as follows; CD31, physoxia (148 MFI) vs. air (26 MFI), vs, CD56, (air 15.9 and physoxia 25 MFI respectively ***p<0.01, CD146, physoxia (744 MFI) vs. air (408 MFI) p<0.05, CD209 CD326, physoxia (788 MFI) vs. air (636 MFI)**P<0.03, CD44 air (101 MFI) and physoxia (77 MFI) for physoxia. CD2 and CD44 displayed an opposite trend to the above noting the negligible expression levels of the latter (CD2 air 41 MFI, physoxia 5.1 MFI, CD44 air 39MFI and physoxia 1.3MFI*P<0.05), HLA-1(air 55MFI and physoxia 81 MFI *P<0.05) and HLA-2 all displayed upregulated expression in physoxia 11 MFI vs. air oxygen 77MFI (P<0.05) in crude EVs. T cell-specific EV markers were significantly higher for C.EVs in the following conditions: CD1c air 81 MFI vs 29MFI physoxia *p<0.05, CD14 air 91MFI

vs physoxia 388 MFI **p<0.04 and CD25 ai 21 MFI vs physoxia 101 MFI **p<0.04. specific B cell EV markers observed on TNC C.EVs were significantly different for CD19 air 33MFI vs physoxia 345 MFI *p<0.05 and for CD2; air 88MFI vs 754MFI at physoxia*p>0.05. **B cell markers** like **CD20 and CD40** are upregulated in air oxygen S.EVs. Tenocyte-derived S.EVs displayed higher levels of immune cell-related surface markers than C.EVs for air and physoxia as a general observation. Except CD31 remained within 5 points over the biological replicates irrespective of culture conditions (figure 6D). Differences in S.EVs at air vs physoxia are as follows. CD146 air 444 MFI vs physoxia 742MFI *p<0.05, CD209,air 128 MFI vs physoxia 354MFI *p<0.05, and HLA 1 air 403 MFI vs physoxia 744MFI *p<0.05. (Figure 6D) In contrast to the general observation of physoxia increasing immune-associated marker express levels on TNC EVs, CD56 was upregulated in air 204 vs. physoxia 101MFI *p<0.05 Analysis of S.EVs B cell marker expression indicated upregulation of CD20 and CD40 in air oxygen, little or no expression of CD45 (in contrast to crude EVs), and marked upregulation of both CD19 33and CD24 in physoxia; CD24 displayed the highest level of expression in S. EV samples at physoxia (Figure 6D). T-cell marker expression in C.EVs displayed upregulation in physoxia of CD14, CD69, and CD25. S.EVs demonstrated the upregulation of CD25 and CD69 in physoxia and marked upregulation in air oxygen of CD14. Expression of CD1c was comparable across all conditions and degree of 3purity of EVs (Figure 6C). CD19 and CD24 are markedly upregulated in physoxia S.EVs. T cell marker expression in C.EVs shows upregulation of CD14, CD69, and CD25 in physoxia. S.EVs show upregulation of CD25 and CD69 in physoxia and CD14 in air oxygen. Increased fractionation to small EVs generally increases the detectable levels of most EV surface markers, irrespective of oxygen conditions. These findings indicate that oxygen levels during tenocyte culture significantly impact the surface marker profiles of the released EVs.The increased expression of stem cell markers in physoxia EVs could indicate a greater regenerative potential of EVs produced under these conditions. The changes in immune-associated markers suggest that oxygen tension can modulate the immunomodulatory capacity of tenocyte-derived EVs. These differences could be important in designing targeted therapeutic strategies using tenocyte EVs, especially in tendon repair where modulation of the inflammatory and regenerative processes are required. In summary, tenocyte EVs exhibit distinct surface marker profiles depending on whether the parent cells are cultured under physoxia or air oxygen conditions. Physoxia promotes the expression of stem cell-related markers, while air oxygen increases certain immune-related markers, highlighting the critical role of oxygen in modulating EV characteristics.

3.*Cytokine Profiles in Tenocyte Conditioned Media and Extracellular Vesicle subgroups at air and physoxia.*

To comprehensively characterize the influence of oxygen levels on tenocyte secretome, we quantified the concentrations of GM-CSF, IFNγ, IL-1α, IL-1RA, IL-1β, IL-2, IL-4, IL-6, IL-8, IL-10, IL-12, IL-18, and TNFα in Tenocyte Conditioned Media (TNC CM), Crude Extracellular Vesicles (C.EVs), and Small Extracellular Vesicles (S.EVs). Generally, tenocyte extracellular vesicle (EV) cytokine profiles were significantly influenced by the oxygen tension during cell culture, with physoxia (2% O2 referred to as“ physoxia”) promoted increases in anti-inflammatory and regulatory cytokines, while normoxia (21% O2, referred to as "air oxygen") resulted in higher levels of several pro-inflammatory cytokines. It is important to note that the observed decrease in cytokine concentrations from TNC CM to C.EVs and S.EVs (Figure 7.A, B, C) reflects the partitioning and enrichment of specific cytokines within different fractions during the EV isolation process, rather than a general reduction in cytokine content within the vesicles themselves. The density gradient ultracentrifugation method selectively separates EVs from soluble proteins and other cellular debris, leading to a concentration of vesicle-associated or lumenal cytokines in the EV fractions, and a removal of soluble cytokines.

3.1. Tenocyte Conditioned Media (TNC CM)

Normoxia (21% O2): TNC CM derived from cells cultured under normoxic conditions exhibited significantly higher levels of several pro-inflammatory cytokines compared to physoxia-derived CM

(Figure 7A). Notably, IFNγ, IL-18, TNFα, and GM-CSF were elevated. Specific examples include: IFNγ (1100 pg/mL vs. 850 pg/mL in physoxia, $p<0.05$), IL-18 (756 pg/mL vs. 550 pg/mL in physoxia, $p<0.05$), TNFα (103 pg/mL vs. 65 pg/mL in physoxia), and GM-CSF (10 pg/mL vs. 0.55 pg/mL in physoxia). Additionally, normoxia led to significantly higher levels of IL-8 (896 pg/mL vs. 795 pg/mL in physoxia, $p<0.05$) and IL-1β (20 pg/mL vs. 10 pg/mL in physoxia), as well as increased IL-12 and IL-4. Conversely, lower levels of anti-inflammatory/regulatory cytokines such as IL-1α, IL-1RA, and IL-10 (e.g., IL-10 at 0.5 pg/mL vs. 80 pg/mL in physoxia, $p<0.05$) were observed under normoxia. Higher levels of IL-2 and IL-1β were also noted in normoxic TNC CM.

Physoxia (2% O2): Conversely, physoxia-derived TNC CM demonstrated increased levels of anti-inflammatory and regulatory cytokines (Figure 7A). For instance, IL-10 and IL-2 (40 pg/mL vs. 12 pg/mL in normoxia, $p<0.05$) were elevated. IL-4 also showed significantly higher levels (12 pg/mL vs. 0.5 pg/mL in normoxia, $p<0.05$). Furthermore, increased levels of IL-1α and IL-1RA were consistently observed across all biological replicates cultured in physoxia, along with lower levels of pro-inflammatory cytokines such as IL-1β, TNFα, GM-CSF, and IL-18.

3.2. Crude EVs (C.EVs); The cytokine profiles within C.EVs also reflected distinct oxygen-dependent patterns (Figure 7B).

Normoxia (21% O2): Markedly higher levels of the inflammatory cytokine IL-8 were observed in normoxia-derived C.EVs, demonstrating a five-fold increase compared to physoxia (3001 pg/mL vs. 798 pg/mL, $p<0.05$). Elevated levels of IL-6 (100 pg/mL vs. 50 pg/mL in physoxia, $p<0.05$), IFNγ (100 pg/mL vs. 83 pg/mL in physoxia), IL-12 (50 pg/mL vs. 30 pg/mL in physoxia), and IL-2 (113 pg/mL vs. 7 pg/mL in physoxia, $p<0.05$) were also present. This suggests a pro-inflammatory phenotype for normoxia-derived C.EVs. IL-18 displayed comparable levels across normoxia (255 pg/mL) and physoxia (230 pg/mL, $p<0.05$).

Physoxia (2% O2): Physoxia-derived C.EVs exhibited higher levels of anti-inflammatory/regulatory cytokines, specifically IL-10 (88 pg/mL vs. 38 pg/mL in normoxia) and IL-1α (8 pg/mL vs. 1 pg/mL in normoxia, $p<0.05$). Concurrently, lower levels of inflammatory cytokines such as IL-8, IL-6, IL-2, and IL-12 were observed when compared to C.EVs from normoxic tenocytes. Overall, these findings suggest that oxygen tension exerts distinct effects on cytokine profiles within C.EV subpopulations, with normoxia generally triggering higher levels of inflammatory cytokines and physoxia promoting regulatory and anti-inflammatory cytokines.

3.3. Small EVs (S.EVs); Small EVs (S.EVs) generally contained the lowest overall concentrations of cytokines compared to TNC CM and C.EVs (Figure 7C).

Normoxia (21% O2): S.EVs from normoxic conditions showed elevated levels of inflammatory cytokines, including IFNγ (97 pg/mL vs. 25 pg/mL in physoxia, $p<0.05$) and IL-18 (45 pg/mL vs. 5 pg/mL in physoxia, $p<0.05$), and TNFα (13.1 pg/mL vs. 8.2 pg/mL in physoxia, $p<0.05$). Conversely, levels of regulatory/inflammatory cytokines such as IL-1α (1 pg/mL vs. 11.9 pg/mL in physoxia, $p<0.05$), GM-CSF (1 pg/mL vs. 12 pg/mL in physoxia, $p<0.05$), IL-6 (2 pg/mL vs. 18 pg/mL in physoxia, $p<0.05$), IL-4, and IL-1RA (1 pg/mL vs. 11.9 pg/mL in physoxia, $p<0.05$) were decreased compared to physoxia.

Physoxia (2% O2): S.EVs derived under physoxic conditions displayed increased levels of regulatory/inflammatory cytokines. Specifically, IL-1α (60 pg/mL vs. 15 pg/mL in normoxia, $p<0.05$), IL-4 (16 pg/mL vs. 90 pg/mL in normoxia, $p<0.05$), GM-CSF (12 pg/mL vs. 1 pg/mL in normoxia, $p<0.05$), IL-6 (18 pg/mL vs. 2 pg/mL in normoxia), and IL-1RA (60 pg/mL vs. 15 pg/mL in normoxia, $p<0.05$) were significantly higher. A non-significant increase in the anti-inflammatory cytokine IL-10 was also observed (9 pg/mL vs. 2 pg/mL in normoxia), following the trend seen in other physoxia-derived secretome subgroups with lower levels of inflammatory cytokines.

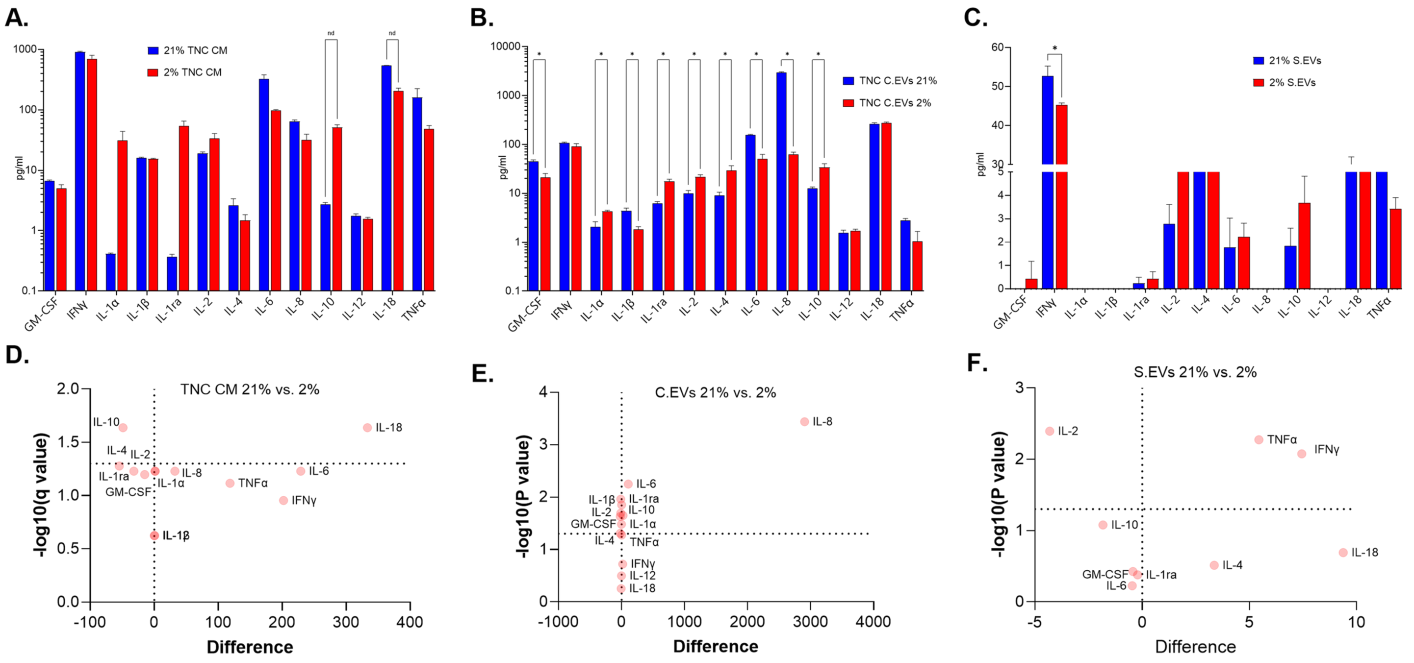


Figure 7: Cytokine and chemokine profiles of TNC-derived conditioned media and extracellular vesicles under different oxygen concentrations. Panels A, B, and C are bar graphs showing the concentration (pg/mL) of various cytokines and chemokines in A) Total Nucleated Cells Conditioned Medium (TNC CM), B) TNC-derived Conditioned Extracellular Vesicles (TNC C.EVs), and C) TNC-derived Small Extracellular Vesicles (TNC S.EVs). The red bars represent the 21% oxygen condition, and the blue bars represent the 2% oxygen condition. Data are presented as mean ± SEM. Asterisks (*) indicate statistical significance ($p < 0.05$). Panels D, E, and F are volcano plots corresponding to the data in A, B, and C, respectively. These plots visualize the difference in concentration (x-axis) and the statistical significance (-log10(q value) or -log10(adjusted P value) on the y-axis) between the 21% and 2% oxygen conditions. Each dot represents a specific cytokine.

3. Discussion.

Tendinopathy is a painful, troublesome and common pathology and makes up to 30% of all primary care consultants in the UK currently(Canosa-Carro et al., 2022).Tendinopathy is still gravely misunderstood and the exact definition of the term of still unclear, currently tendinopathy is diagnosed as a clinical hypothesis based on symptoms and patients physical limitations. The pathophysiology appears to relate to disorganization within the structure of the tendon, however there is a discrepancy between patient imaging and clinical symptoms, for example many asymptomatic subjects display disorgonisation and symptom free subjects display apparently “normal” tendons.

Despite advances in tendon research to date no treatment/ curative agent exists, management of symptoms via medical, physical therapy and eventually surgical repairs. Tendons reside at a lower oxygen concentration than that of bone, muscle and many other tissues of the body due to lower levels of vascularisation of the tendon partial oxygen pressures observed in human tendons is between 2-5%. Oxygen consumption in tendon is 7.5 times lower than skeletal muscle, demonstrating the need for tenocyte specific physiological oxygen levels during cell culture (often termed hypoxia when describing cells with physiological oxygen requirements at around 15-19 % eg; Mesenchymal stem cells). Extra cellular vesicle field has grown exponentially over the last 25 years and the EVs from many cell types have been explored as indicators of disease and potential treatments, however the current exploration of tendon extra cellular vesicles is extremely limited to date with only a handful of fundamental studies. EVs present a potential non invasive treatment and a potential biomarker for tendinopathy, they have an excellent safety profile and stable shelf life up to 2 years at

room temperature with no deterioration of the internal and external proteins("Correction to 'Minimal Information for Studies of Extracellular Vesicles (MISEV2023): From Basic to Advanced Approaches'(Journal of Extracellular Vesicles, (2024), 13, (E12404), 10.1002/Jev2.12404)," 2024).

3.1.Air oxygen vs physiological oxygen modulation of size, protein and lipid content.

Utilizing oxygen concentration to modulate EV secretion has been adopted within EV manufacturing facilities, research done with mesenchymal stem cells cultured at 2% (hypoxia) oxygen produced significantly more EVs when compared to conventional 21% oxygen, Hypoxia activates the hypoxia inducible factor (HIF) signaling pathway Under normoxic conditions, HIF-α is rapidly hydroxylated by prolyl-4-hydroxylases (PHDs) and directed to proteosomal degradation. When there is hypoxia, however, this degradation process is suppressed, and the HIF-α subunits translocate into the nucleus to bind with HIF-1β (HIF1B). The heterodimeric complex then locates to the hypoxia-responsive elements (HREs) leading to the subsequent upregulation of more than 100 target genes including vascular growth factors VEGF-A and PDGF-B to promote tissue survival. In addition, there are HIF-independent signalling pathways that are also activated under hypoxia; nuclear factor-κB (NF-κB) , mTOR and STAT3 pathways. In 2024 a review on technical aspects of EV research and functions of hypoxic EVs (2%) in comparison to normoxic EVs (21%)(Phelps et al., 2023) In this review, publications were evaluated according to the ISEV minimal reporting guidelines for the cell types covered (MSCs, cancer & cardiovascular), highlighting that outside of these areas little is known regarding oxygenation and its influence on EVs and their cargo and to date the research presented in this report is the first to robustly isolate and characterise tenocyte EVs. The review demonstrates the diverse functional effects of hypoxia-induced EVs across different recipient cell types with promoting angiogenesis, migration, and cell proliferation being the commonly recorded outcomes, however the presence of reoxygenation and the origin of the hypo-EVs adds complexity and this complexity underscores the need for further research to fully elucidate the intricate roles of hypoxic EVs in various physiological and pathological states whilst also demonstrating the lack of research with a focus on TNC EVs. lipids provide EVs with their ability to fuse with membranes to enable biomolecule delivery. Lipids have been identified in EVs in several reports;cholesterol, phosphatidylcholine, phosphatidylserine, and sphingomyelin derivatives are among the most commonly detected, the relative and the absolute values of lipids in the differen tenocyte EV subgroups s provides interesting information regarding oxygenation during collection and the resulting lipid content of TNC EVs, physiological oxygen (2%) levels used to culture parent cells produced EVs with higher lipid levels than traditional 21% oxygen during culture.These differences warrent futher exploration in order to define the specific composition of lipids present. Crude EVs collected in physoxia contained significantly higher levels of IL-8 when compared to air oxygen derived TNC EVs This difference in IL-8 levels between crude and pure EVs can be explained by the way ultra-centrifugation concentrates any vesicles-cytokine complexes present in CM (Figure 7A).

3.2. EV isolation method influences physical and chemical characteristics of tenocyte EVs.

Most EV separation techniques utilised in experimental settings create challenges in delineating which component(s) deliver the biological effect, or otherwise.(Crescitelli et al., 2021). To date only one in vivo animal study where TDSC EVs were used in a mouse model of acute achillies trauma(Kasula et al., 2024) the injury group treated with TDSC EVs relieved the expression of MMP3 and elevated expression of TIMP3, Col-1a1 and TNMD, which balanced and maintained the homoeostasis of tendon. At the same time, the biomechanical properties of the injury tendon were improved by EVs. However the isolation and characterisation of the EVs did not fully align with minimal reporting guidelines from ISEV(supplementary table 4). One rabit study using a lyopholised EV preparation showed some histological improvements and reduction in adhesion formation in the group treated with EVs and although the study is promising, the composition and or characterisation of the EV preparation is not discussed in the methodology and desribed that the exosome preparation has yet to show evidence of inducing tendon regeneration(Wellings et al., 2021). These results do provide a potential proof of concept regarding the exploration of TNC EVs as theraputics and to improve the pathophysiology involved in tendinopathy(Kasula et al., 2024). The methodology used in this work was developed in order to adere to the ISEV standards for EV isolation and charaterisation of extra cellular vesicles(Welsh et al., 2024) the majority or EV papers published have a limited level of reporting in terms of a detailed list of factors that can influence the effect of reported outccomes observed in EV research , MISEV2023 encourages meticulous reporting of experimental details, covering aspects such as nomenclature, pre-processing variables, separation, characterisation of EVs, functional studies, and in vivo analysis of EV release, uptake, and functions.

3.3. Tenocyte cytokine modulation via oxygen concentration during culture.

Oxygen-Dependent Profiles: The oxygen concentration during tenocyte culture significantly influences the cytokine profiles within the EVs, with physoxia promoting anti-inflammatory responses and air oxygen triggering higher levels of inflammatory cytokines.

3.3.1. EV Subtype Differences

Cytokine concentrations vary across tenocyte-derived CM, crude EVs, and small EVs. Small EVs generally contain the lowest overall cytokine concentrations compared to CM and C.EVs. Anti-inflammatory vs. Pro-inflammatory: Physoxia tends to increase the levels of anti-inflammatory cytokines such as IL-10, while air oxygen conditions typically result in higher levels of pro-inflammatory cytokines such as IL-6, IL-8, and TNF-α. IL-8: Notably, air-derived crude EVs displayed a markedly higher level of the inflammatory cytokine IL-8 compared to those derived in physoxia. This may be due to how ultracentrifugation concentrates any vesicle-cytokine complexes in the CM.

3.3.2. Relevance to Tendinopathy

The study indicates the potential for using oxygen levels as a tool to yield specific EV phenotypes with specific cytokine profiles, understanding the impact of oxygen concentration on tenocyte EVs is important because tendinopathy is a common and troublesome condition with a pathophysiology that appears to relate to disorganisation within the structure of the tendon, some cytokines, such as GM-CSF, are found in high levels in joints with tendinopathy. Blocking GM-CSF may reduce inflammation and damage. IL-6 is also involved in human tendon disease and is increased in tendon tears, whereas IL-1β, IL-6, and TNF-α are increased in animal models of tendon injury. These findings suggest that manipulating oxygen levels during tenocyte culture can influence the cytokine composition of EVs. This could have implications for therapeutic strategies using tenocyte-derived EVs to modulate inflammation in conditions like tendinopathy.

3.4. Tenocyte EV surface marker profiles are influenced parent cell oxygen levels during culture:

B cell marker expression displayed a relatively distinct expression profile where C.EVs expression of CD20, CD40, and CD45 was comparable across both culture conditions while CD19 and CD24 were markedly upregulated in physoxia. IL-8 is often found attached to EVs isolated from fibroblasts and blood derived EVs and could explain the presence of IL-8 at higher levels in crude EVS than in CM and pure EVs(Fitzgerald et al., 2018). Interestingly the hypoxia inducible factor-1 (Hif-1) which is upregulated when oxygen concentrations drop bellow a tissues physiological baseline, HIF-1 may play a role in mediating tendinopathy pathogenesis. Previous studies have shown that HIF-1 is significantly upregulated in tendinopathic tendons, where it regulates the expression of pro-inflammatory cytokines, apoptotic mediators, and angiogenesis, exacerbating tendinopathy. Whether the EV associated cytokines reflect the physiological function of EVs or the cytokines themselves is a regulated physiologic process that needs further clarification. To date this is the first documentation of tenocyte EVs isolated and described the follows the minimal reporting guidelines mentioned above, this work will provide a solid foundation for futher exploration and functional studes. This work demonstrates that Hypoxia (physoxia for tendon) and EV biogenesis are complex intertwined processes. Oxygen conncentration is able to modulate EV release through HIF-dependent and -independent mechanisms, altering the EV cargo and their subsequent recipient cells. The functional impact of Hypo-EVs depends on the recipient cell type and the specific experimental conditions. These complex interactions contribute to cellular adaptation to hypoxia and play a role in various physiological and pathological processes, including cancer, cardiovascular diseases, and inflammation

4. Materials and Methods

4.1. Tenocyte isolation and expansion

All tissue used in this work is derived from the food chain. Porcine dorsal flexor tendons were isolated from the trotters of three. female, 12-month-old pigs, 72 hours post-slaughter. The paratenon was removed and the tissue treated with two separate antibiotic washes (Penicillin, streptomycin, and amphotericin (PSA), at a 10X concentration in phosphate buffered saline for 10 minutes. The

tendon tissue was dissected by hand into approximately 1mm². in size, with Swann Morton scalpel blade (No 26) and a No.4 handle. 6 well tissue culture plates (Greiner bio one) were scored with the blade described above, score lines projected laterally from the center of the well to improve cell migration out from the tissue and improved adherence of the tissue to the plastic. Tissue sections were added to the central point in the well plate before

Leaving the tissue containing plate in the biosafety cabinet with no lid for 10 minutes before the addition of medium to improve the chances of the tissue remaining adhered to the plastic during media addition. Dulbecco's Minimal Essential Medium (DMEM, Lonza), supplemented with 10% fetal bovine serum (Cytiva), 1% PSA, 1% L-glutamine (Lonza) and 1% non-essential amino acids (Lonza). All cultures were maintained throughout in a 21% O2 air oxygen incubator or a 2% O2 tri gas incubator. Emerging cells begin appearing from 2-4 days , throughout culture media was changed every 3 days until wells reached approximately 70% confluency, passage was carried out enzymatically via trypsin/EDTA in 1X (10µg/ml) concentration, diluted with sterile PBS (Lonza and placed in the appropriate incubator (2% or 21% O² for approximately 15-20 mins). An equivalent dose of growth medium was added to inhibit the trypsin. Detached cells were removed from tissue culture flask and added to a 50ml falcon tube and spun 500g for 3 minutes. The resulting pellet was resuspended in 4 ml of media, before viability and cell number were obtained via trypan blue. Cell density of 2 x 10^4/cm² was used for both standard air oxygen (21% O2) and reduced physoxia (2% O2) conditions in a tri-gas incubator. Cumulative population doublings were determined by serial cell counts from passage 1 to passage 12.

4.2. Cell resurrection and maintenance: Mesenchymal stem cells and tenocytes.

Human cryopreserved mesenchymal stem cells from three separate donors used in this work were isolated from a commercial fully characterised bone marrow aspirate (10ml) cryopreserved at passage 2, method described in detail in Kaye et el 2015. after 12 months in liquid nitrogen. Cryovials' were immediately thawed in a 37 °c water bath over 2 minutes during this time the vials were kept under gentle agitation to prevent uneven thawing and thawed cell suspension adding dropwise into 15 ml of pre warmed medium before final transfer into a adherent T75 cell culture flask (Greiner bio one) for recovery. Thawing and subsequent culture of hMSC ampoules were as described above. MSCs were expanded using the following media composition; Dulbecco Modified Eagle Medium (DMEM, Thermo Fisher) supplemented with 10% (v/v) Foetal Bovine Serum (FBS, Thermo Fisher), 25 millimolar (mM) L0 glutamine (Thermo Fisher), 1% (v/v) non-essential amino acids (NEAA, Thermo Fisher), and 1% (v/v) Penicillin-Streptomycin & amphotericin (Thermo Fisher).

4.3.Tri-lineage differentiation.

Adipogenesis; For adipocyte differentiation, MSCs were reseeded a density of 2000 cell/cm2 and were switched to adipocyte induction medium, consisting of DMEM basal medium supplemented with 10% FBS, 0.5 mM 3-isobutyl-1-methylxanthine (IBMX), 100 µM Indomethacin, 1 µM Dexamethasone, 10 µg/ml Insulin, with media changed every 3 days. After 21 days of induction, cells were fixed in 4% paraformaldehyde and stained with Oil Red O solution.

Osteogenesis: For osteoblast differentiation, MSCs were reseeded a density of 2000 cell/cm2 and switched to osteogenic induction medium, consisting of HG-DMEM basal medium supplemented with 10% FBS, 50µg/ml L-Ascorbic acid, 0.1 µM Dexamethasone, 10 mM β-glycerophosphate, 1 mM Sodium pyruvate, with medium change every 3 days. After 21 days of induction, cells were fixed in 4% paraformaldehyde and stained with Alizarin Red S solution.

Chondrogenesis; For chondrocyte differentiation, MSCs were reseeded a density of 2000 cell/cm2 and switched to chondrocyte induction medium, consisting of LG-DMEM basal medium supplemented with 10% FBS, 50 µg/ml L-Ascorbic acid, 0.1 µM Dexamethasone, 10 ng/ml TGFβ3, 1 mM Sodium pyruvate, 1X Insulin-Transferrin-Selenium solution, with medium change every 3 days.

After 21 days of induction, cells were fixed in 4% paraformaldehyde and stained with Alcian blue solution.(Kay et al., 2015)

4.4. Tenocyte and Mesenchymal stem cell characterisation via surface marker profiles via single stain Flow cytometry.

The resulting cell suspension was centrifuged at 500g for 5 minutes, resuspended in 1 ml of media and counted. A total count of 250,000 cells was added to an Eppendorf tube, 2 ul of PE conjugated antibodies added, volume made up to 100 ul (with FACS buffer) and incubated for 30 minutes in the dark. FACS buffer, 1 ml, (PBS, 2% FCS, 2mM EDTA) was added and the tube centrifuged for 10 minutes at 500g. The FACs buffer was removed from the pellet and stained cells were resuspended in 200ul PBS. Cytoflex cytometer (BD Biosciences, San Jose, CA) was used for sample analysis and data recorded for the PE and FITC channels. All analyses were performed using FlowJo software (BD Biosciences, San Jose, CA). Univariate distributions of flow cytometric data from cells stained with and the corresponding isotype control were compared by probability binning in 300 bins using FlowJo software, to obtain the T(x) metric.

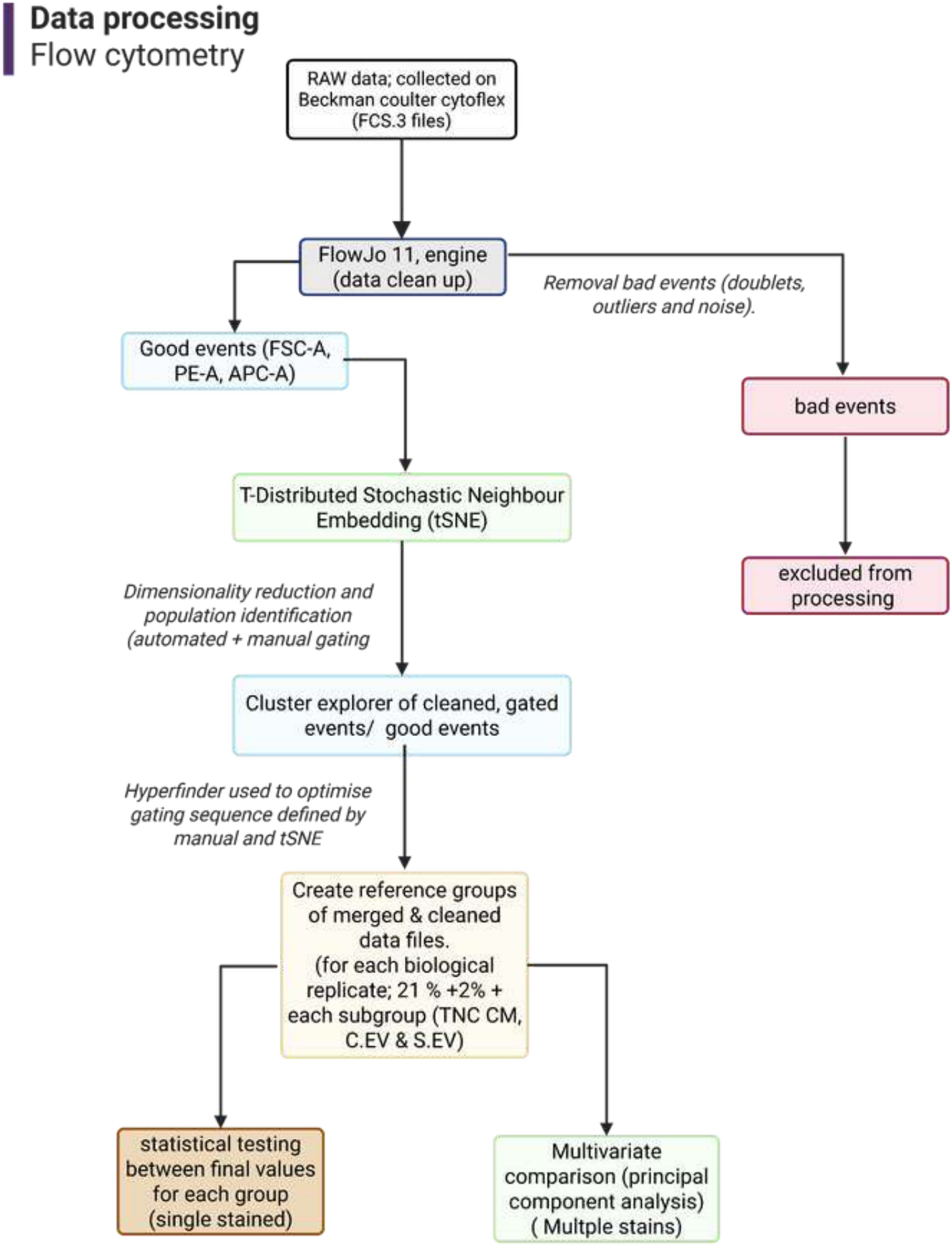


Figure 8. flow cytometry data processing flow chart for single stained and multiple stained samples.

4.3.2 Immunofluorescence

All samples were fixed with 4% paraformaldehyde in PBS for 30 minutes and washed with PBS before the addition of anti-goat tenomodulin (Abcam; dilution 1:100) for 24 hrs. at 4°C. After washing with PBS samples were incubated with secondary antibody (conjugated with Alexa Fluor 488, Thermo Fisher Scientific) and the nuclei counterstain DAPI for 2 hours, protected from light, at room temperature. Image acquisition was undertaken at 20x magnification, and the images converted to TIF format using OlyVIA Desktop software using DX83 Olympus fluorescence microscope.

4.4 Secretome collection and fractionation;

Conditioned media collection and characterisation; Tenocyte conditioned media collection: cell-conditioned media (600–1200 ml) from 70% confluent Tenocyte cells grown in T175 cell culture flasks, (3.5 × 104 cells/cm2) the expanded cells for each biological replicate (P1-P5) were monitored for the following; any changes in morphology, contamination (regular mycoplasma testing), drastic changes in proliferation via regular cell counts and viability assessments after the removal of CM. Total cell number was obtained for each vessel (see supplementary data 6.2 for detailed cell health monitoring data). Before transfer to 50ml tubes all TNC CM media underwent filtration to remove any dead cells/protein fragments/cellular debris by passing through a 0.22µm sterile syringe before freezing (-20) for a maximum of 3 months. Protein concentration was determined for all samples pre and post thaw to asses the freeze thaw process on protein content and as a crude proxy for the presence of EVs (supplementary data 6.4).

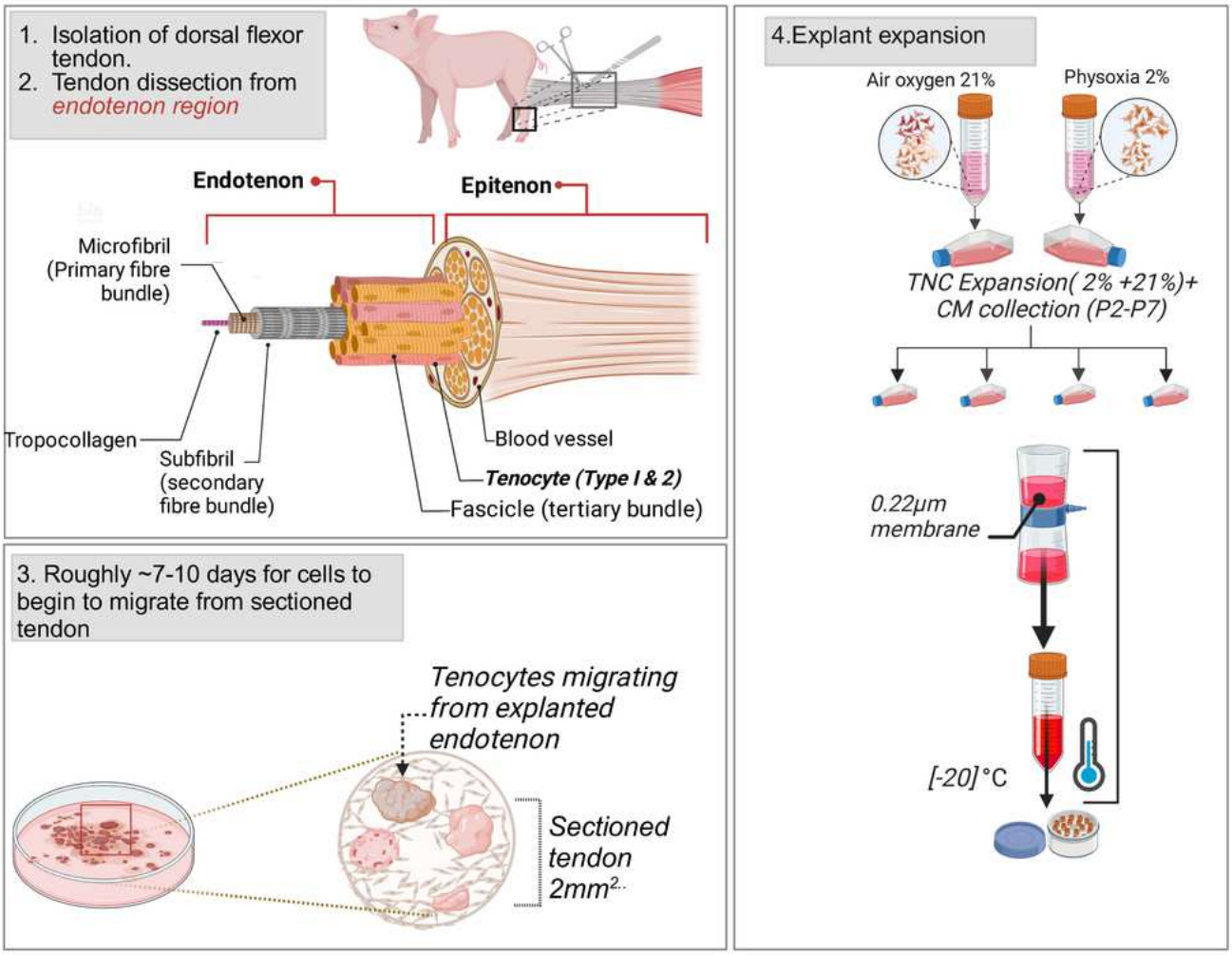


*Figure 9. Isolation, Dissection, and Expansion of Tenocytes. This schematic diagram illustrates the sequential steps for isolating, dissecting, and expanding tenocytes for in vitro research. The process begins with the **isolation of the dorsal flexor tendon** from a porcine model*

*(Step 1). Following isolation, the tendon is subjected to **dissection from the endotenon region** (Step 2). The diagram highlights the hierarchical structure of the tendon, showing the outermost layer, the **epitenon**, and the inner connective tissue, the **endotenon**. Key structural components are indicated: *Fascicle (tertiary bundle):** A grouping of smaller fiber bundles. *Blood vessel:** Shown supplying the tendon tissue. Tenocyte (Type I & II):** The resident cells of the tendon. Subfasicle (secondary fibre bundle):** A bundle within the fascicle. Microfibril (primary fibre bundle):** The basic unit composed of **Tropocollagen**.*

*The dissected tendon is sectioned into small pieces, approximately **2mm^2**, and placed in a culture dish to undergo explant culture. **Tenocytes begin to migrate from the sectioned tendon and explanted endotenon** after roughly **7–10 days** (Step 3). The inset micrograph visually represents tenocytes migrating out of the tendon tissue onto the culture surface. Following migration, the tenocytes are harvested and cultured under two distinct conditions for **Explant expansion** (Step 4): 1. **Air oxygen (21%):** Standard atmospheric oxygen concentration. 2. **Physoxia (2%):** A reduced oxygen concentration, mimicking the physiological environment. Both conditions are used for **Tenocyte (TNC) Expansion** across passages **P2–P7** (TNC Expansion ($2\% + 21\%$) + CM collection (P2–P7)), with the goal of expanding the cell population while also **collecting conditioned medium (CM)** from the cultures for subsequent analyses. The resulting expanded cell cultures are shown being distributed into multiple flasks.*

4.5. Isolation of tenocyte extracellular vesicles from conditioned media.

Methods used to isolate TNC EV subgroups from conditioned medium adhered to ISEV recommendations described byRoyo et el, for each TNC EV preparation obtained had been subject to the following; TNC EV subgroups stated in this work were defined by multiple quantitative measures of size & density and each subgroup also used multiple techniques in order to define abundance of EVs (total particle number and/or protein or lipid content).Each group was also tested for the presence of components associated with EV subtypes (Tetraspannins; CD8, CD9 &CD63) and for the presence of non-vesicular, co-isolated components (Cytokine analysis for all EV preparations and controls for 12 different cytokines).

CM was centrifuged at 100,000g for 90 minutes (SW 41 Ti rotor and Optima XPN ultracentrifuge, Beckman Coulter), the supernatant removed, and the resulting crude EV pellet resuspended in 500 µl of PBS, Small EVs were obtained via further fractionation of C.EV samples using size and density as proxies to isolate SEVs (20-500nm) by a bottom up iodixanol density gradient was freshhly prepared for each EV sample; Density gradient medium: 60% iodixanol in distilled water (OptiPrep™, Axis-Shield) 40, 20,10 and 5%w/V% iodixanol solutions. Working solution: 0.25M sucrose, 6mM EDTA, 60mM Tris-HCl; pH 7.4. Homogenization medium: 0.25M sucrose, 1mM EDTA, 10mM Tris-HCl; pH 7.4. Gentle addition of the base layer of the gradient solution (40% iodoxional, estimated density ~1.224 g/ml) to a 14 × 89 mm thinwall, ultra-Clear™ tube (Beckman Coulter, Brea, USA, #103277) follwed by the 20, 10, 5 % soltions (with densities from 1.12 to 1.19g/ml) in an Optima XPN-80 ultracentrifuge with a swinging bucket SW32.1 Ti rotor (Beckman Coulter, *k*-force: 3571 and 357.1) at maximal brake. at 120,000g for 18 hours. 12 individual 1ml fractions Small EVs have a density of ~1.13 - 1.17 g/ml and will migrate to fractions 4 - 7 (Iwai et al., 2017)., These fractions were pooled, resuspended in PBS, and centrifuged at 120,000g for 2 hours at 4°c to remove residual sucrose and Iodixanol. Washed pellets were resuspended in 500ul of PBS before downstream validation of protein and lipid concentrations finally S.EV samples were at -20°C for a maximum of 6 weeks, on thawing protein and lipid concentrations were determined before any EV functioanl/characterisation experimental procedures (Figure 9).

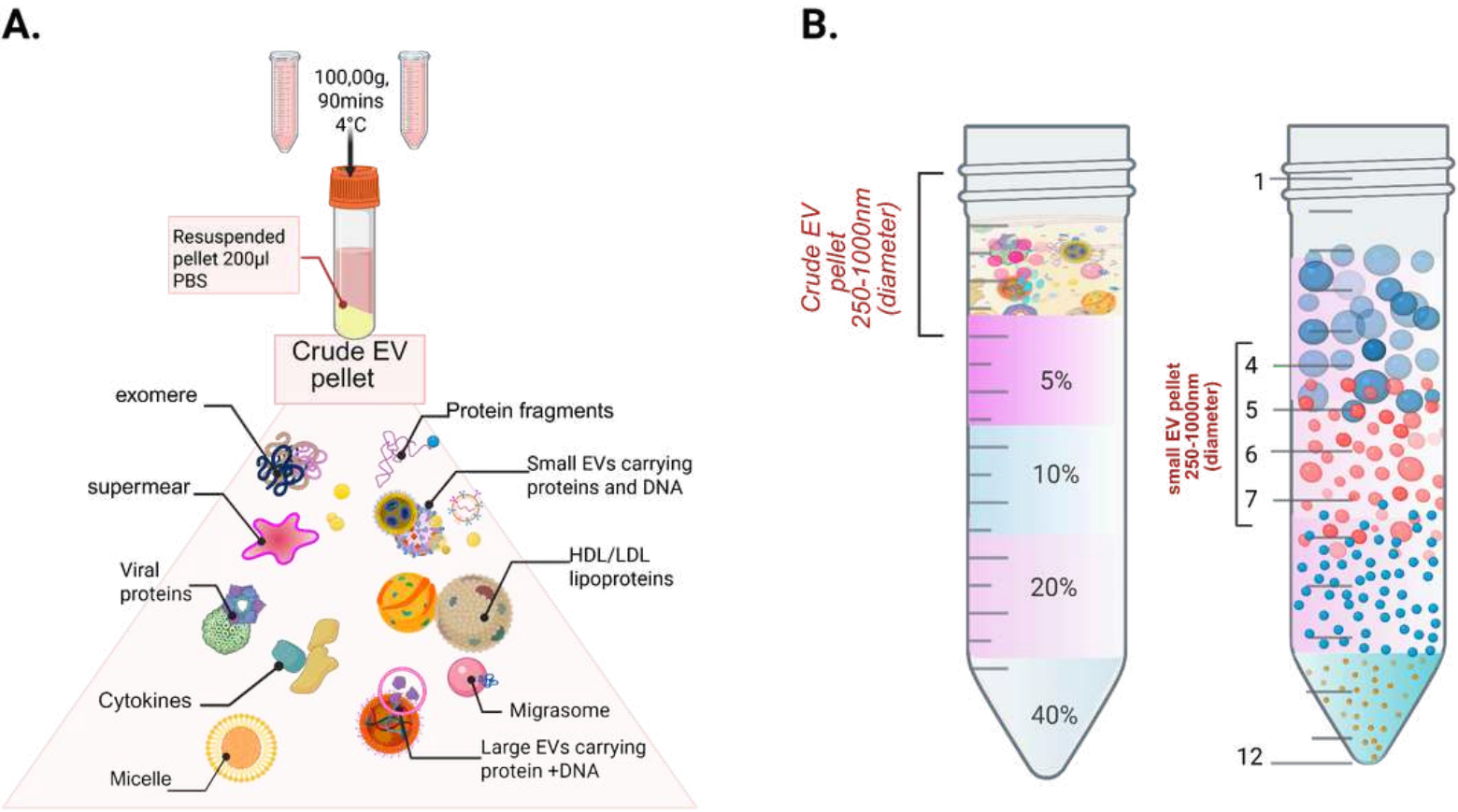


Figure 10 . Extracellular Vesicle (EV) Isolation and Separation Methodology.(A) Crude EV Pellet Isolation and Composition: This schematic illustrates the generation of a crude EV pellet via ultracentrifugation at 100,000 x g for 90 minutes at 4°C. The resulting pellet, resuspended in 200 µL of PBS, is heterogeneous, containing a mixture of vesicles and other biological components. These components include various types of EVs (e.g., "exomeres," "supermear," small EVs carrying proteins and DNA, large EVs carrying protein + DNA), as well as non-EV contaminants such as protein fragments, viral proteins, cytokines, micelles, HDL/LDL lipoproteins, and migrasomes.(B) Density Gradient Ultracentrifugation for EV Sub fractionation: This panel depicts the subsequent separation of the crude EV pellet using a sucrose or iodixanol density gradient. The left tube shows a typical gradient (e.g., 5%, 10%, 20%, 40%) used for separating particles based on their buoyant density. The right tube illustrates the expected distribution of different EV populations and contaminants within the gradient. "Crude EV pellet (250-1000nm diameter)" refers to the initial, heterogeneous pellet. The "small EV pellet (25-1000nm diameter)" indicates a more purified fraction often containing exosome-like vesicles. The different colored spheres represent various particles, with distinct populations settling into specific density fractions (e.g., fractions 4-7 often enriched for small EVs, while larger vesicles, lipoproteins, and protein aggregates may reside in other fractions).

4.2.0.TNC EV Characterization.

Characterization is challenged by small particle size, heterogeneity of EV size and molecular heterogeneity, a lack of universal EV identification methods, and the non-EV-specificity of many measurement techniques. As a result, no single measurement or method can satisfy all EV characterization requirements, and the use of orthogonal methods (those that do not have the same measurement limitations) is recommended. EVs have a particulate structure and contain proteins, lipids, nucleic acids, and other biomolecules. Quantification of each of these components described in this work should be used as a proxy for quantification of TNC EVs and that these values may not directly correlate with EV numbers.

4.2.1 size determination; SEM and particle size measurements.

Absolute EV sizing and counting methods are currently imperfect and will require further improvement, aided by appropriate EV reference standards that are now in development. Nevertheless, current methods can provide a reasonable indication of particles per volume and

particle size distributions that are best interpreted when combined with general characterization. Sizes values for all EV subgroups and controls (DMEM) obtained using a combination of Dynamic light scattering (DLS), SEM and TEM size measurements to validate size data from each technique. To attach size values with function the following cut off based on ISEV guidance were as follows; small EVs defined as a particle diameter of between 20-500nm, large EVs 500-1000nm and for values >1000nm the definition(Welsh et al., 2024). For DLS a NanoE zetasizer (Malvern Instruments). EV samples were diluted with filtered PBS (1:100). Size parameters were established via the zetasizers built in quality control system to avoid inaccuracies due to concentration effects. To determine optimal volumes/concentrations EVs a series of dilutions based on protein concentration ranging from 10µg/ml up to 500µg/ml diluted with DMEM at a volume of 500µl using a standard 12mm o.d. square disposable polystyrene cuvette, for diameter, polydispersity values followed the same procedure using a lower volume 60µl in a DTS1070 cuvette.

Samples for SEM were prepared by adding sample to adhesive carbon pads and allowing the liquid to evaporate over night before the application of a gold splutter coating was applied to prevent charging of the specimens and to increase the amount of secondary electron detection. Thickness of gold splutter layering applied was between 2–20 nm, splutter coating and image acquisition was undertaken by Dr T Hashimoto, Henry Royce Institute, University of Manchester. Images acquired on Quanta 250 FEG scanning electron microscope with Gatan 3View attachment for serial block face imaging and analysis of all TNC secretome samples at air, physoxia and their corresponding subgroups for all biological replicates. Measurements obtained were surface area, vesicle diameter and width of particles present, analysis was via Mountains SEM analysis software(*Digital Surf - Surface Imaging, Analysis and Metrology Software*, n.d.). EV sizes were grouped based on the current size and nomenclature of ISEV; Large were defined as any vesicle between 1000-500 nm, and small EVs include any vesicle between 20-500 nm(Royo et al., 2020)

.

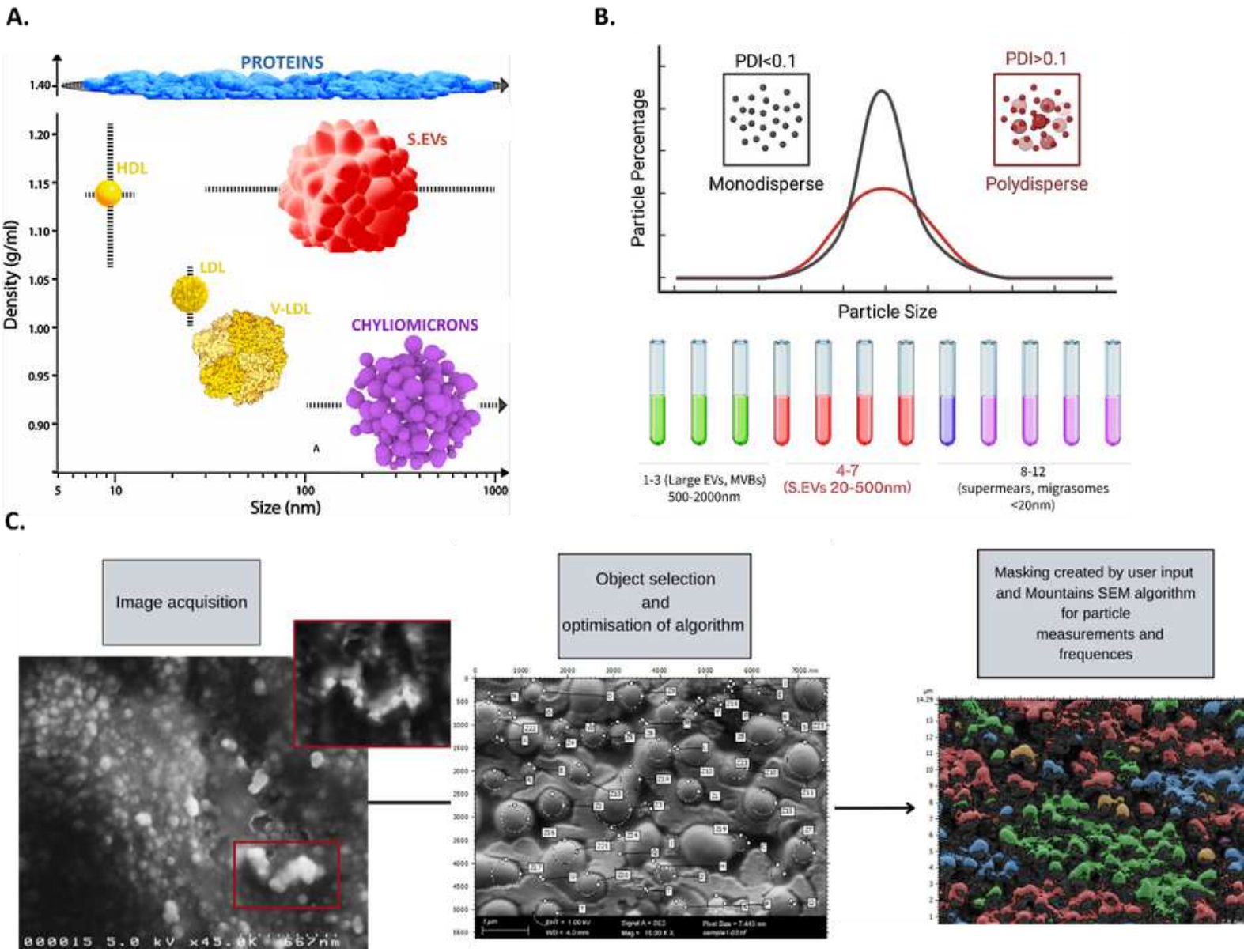


*Figure 11. Characterization of Extracellular Vesicles (EVs) by Density, Size, and Morphological Analysis.(A) Density and Size Distribution of EVs and Lipoproteins: This schematic illustrates the typical density and size ranges of various components found in biological fluids, particularly relevant during EV isolation. Proteins are found at densities typically above 1.20 g/mL, with varying sizes. High-density lipoproteins (HDL) are around 1.15 g/mL, low-density lipoproteins (LDL) around 1.05 g/mL, and very-low-density lipoproteins (V-LDL) and chylomicrons at lower densities (e.g., 0.95-1.00 g/mL). Small EVs (S.EVs) are shown with a density range overlapping with proteins and lipoproteins (around 1.10-1.20 g/mL) and a size range typically between 30 and 150 nm, while larger vesicles (not explicitly labeled but inferred from context) and other components like chylomicrons span up to 1000 nm in size. This panel highlights the challenge of separating EVs from contaminating lipoproteins and proteins based solely on density. (B) Particle Size Distribution and Polydispersity Index (PDI): This panel demonstrates how particle size distribution is analyzed, likely using techniques such as Nanoparticle Tracking Analysis (NTA) or Dynamic Light Scattering (DLS). The graph shows two representative particle size distributions: a monodisperse sample (PDI < 0.1, indicating a narrow size range) and a polydisperse sample (PDI > 0.1, indicating a broad size range). Below the graph, a series of tubes (1-12) suggests fractions obtained from a separation process (e.g., density gradient as shown in Figure 9B), with typical EV populations indicated for each: "Large EVs, MVBs" (Multivesicular bodies) in fractions 1-3 (500-2000nm), "S.EVs" (Small EVs) in fractions 4-7 (20-500nm), and "supermeas, migrasomes" (<20nm) in fractions 8-12. This illustrates how different EV subpopulations are enriched in specific fractions based on their size and/or buoyant density.(C) Image Analysis Workflow for SEM Data: This flowchart illustrates the steps involved in analyzing scanning electron microscopy (SEM) images for particle measurements and frequency. * Image acquisition: The initial SEM image is captured (left panel), showing raw data with visible particles. Red boxes highlight regions of interest where particles are visible. * Object selection and optimization of algorithm: Image analysis software (e.g., Mountains SEM) is used to automatically identify and outline objects (particles) based on predefined criteria, with manual optimization to ensure accurate detection (middle panel). The overlaid lines and numbers indicate the software's recognition of individual particles. * Masking by user input and Mountains SEM algorithm for particle measurements and frequencies: A final mask is generated, often with user input, to isolate the identified particles. Different colors (e.g., red, green, blue) may represent*

different categories or successful identification, allowing for precise measurement of particle size, shape, and frequency distribution (right panel). This process quantifies morphological characteristics of EVs observed under SEM.

4.3. Protein and lipid ratios.

The protein concentrations of all TNC EV subgroups were assessed using the Bradford assay (Coomassie-Plus – The Better Bradford, Pierce Biotechnology, Inc). Bovine serum albumin (BSA) was used for standard curve generation (0.1 – 1000 ug/ml) standards of 0, 0.1, 0.2, 0.4, 0.8 and 1mg/ml were prepared by dilution of BSA standard stock solution (1mg/ml) with analytical grade H2O to a final volume of 200µl each standard was prepared in triplicate and a standard curve was prepared freshly for each sample tested at each stage of fractionation. Absorbance values were obtained using BioTek Synergy HTX Multimode Microplate Reader S1LFA, at 595 nm for all standards and samples. Background values obtained using 200µl of either un-supplemented DMEM for CM samples and PBS for C.EV and S.EV samples. Absorbance values were subtracted from all sample and standards before plotting the standard curve, 400µl of Bradford/Coomassie solution was added in triplicate for each run as a quality check for a degradation of the reagent. All values are presented as an average with an accompanying standard deviation derived from three technical replicates for a total of 3 biological replicates.

Total lipid was determined via the Sulfo-vanillin assay (unsaturated fatty acid quantification kit, ABCAM, plc, ab242305). Standards were prepared with 100% fish oil/DHEA diluted with DMSO and ranged from 0.1 µg/ml to 500 µg/ml. Experimental groups were TNC CM, TNC crude EVs and TNC small EVs, from both air and physoxia conditions, at a final volume of 100µl volumes. Concentrated sulfuric acid (Sigma-Aldrich, 100034) (50µl) was added to standards and samples heated to 98 ˚C on a hot plate under a fume hood, and left for 30 minutes, to solubilize the EV lipid bilayer. Background values were obtained directly with a plate reader at 430nm.After background acquisition the Sulfo-vanillin reagent was added to each well (10µl) followed by an incubation period of 1 hour at 37˚C. Afterwards, fluorescence values were again obtained at 430nm, to obtained sample fluorescence measurements; background values were subtracted from all wells (samples and standards) to plot a standard curve. Values of TNC CM, crude EVs, pure EVS at 21% and 2% lipid concentration values were calculated via the standard curve, averages and standard deviation obtained for each and expressed as µg/ml (Figure 8).

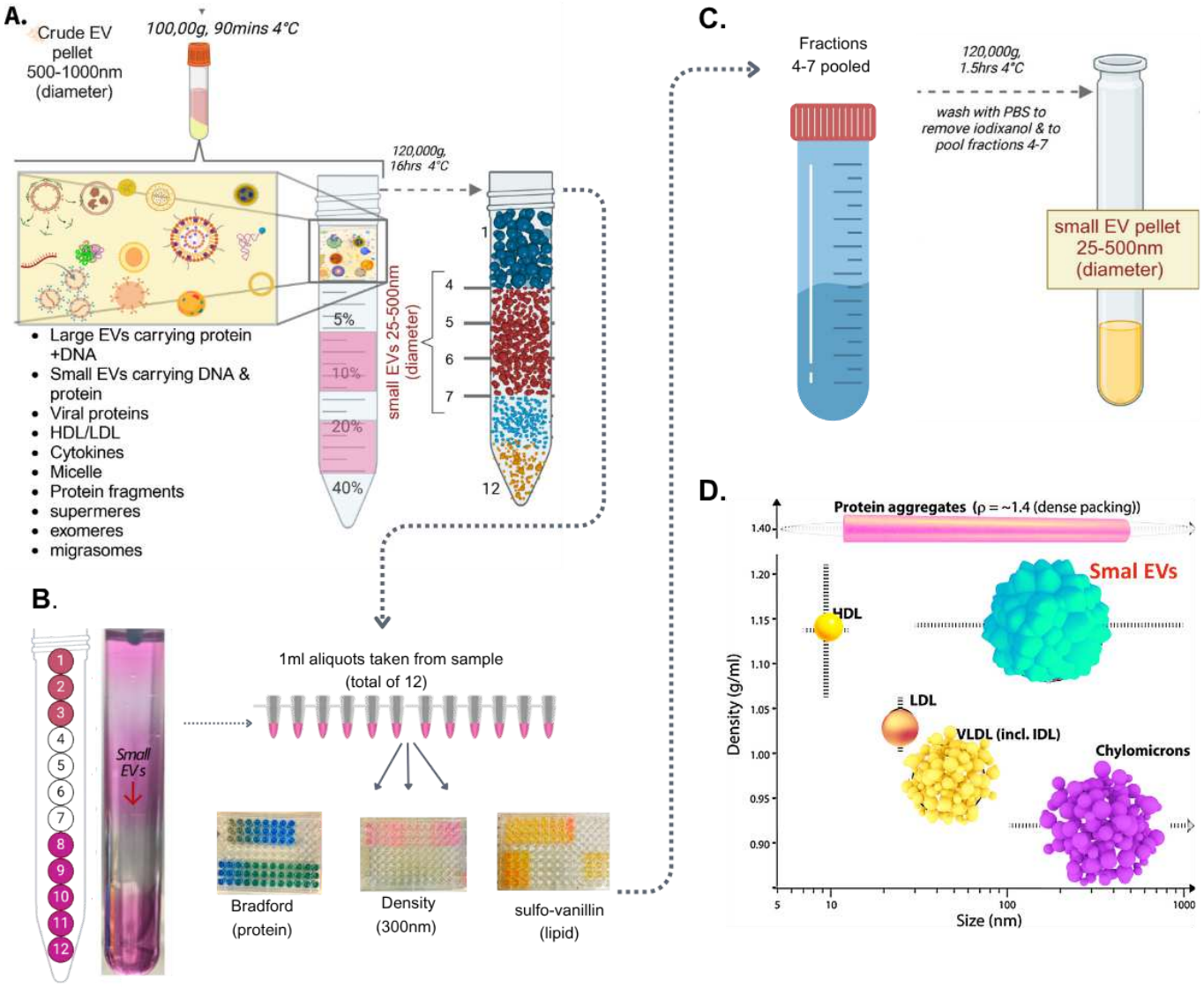


Figure 12. Optimized Workflow for the Isolation and Purification of Small Extracellular Vesicles (S.EVs) via Density Gradient Ultracentrifugation. (A) Isolation of Crude EV Pellet and Initial Density Gradient Separation: This panel illustrates the initial steps of EV isolation and the first stage of purification. A crude EV pellet, containing a heterogeneous mixture of vesicles and other biological components ranging from 500-1000nm in diameter (as indicated on the left), is obtained via ultracentrifugation (e.g., 100,000 x g for 90 minutes at 4°C). This crude pellet is then layered onto a discontinuous density gradient (e.g., 40%, 20%, 10%, 5% indicated on the left tube) for initial separation. The diagram details the expected distribution of various components within the gradient, including large EVs carrying protein + DNA, small EVs carrying DNA & protein, viral proteins, HDL/LDL, cytokines, micelles, protein fragments, supermeres, exomeres, and migrasomes. Following ultracentrifugation (120,000 x g, 16 hours, 4°C), the gradient separates into distinct bands, with "small EVs 25-500nm" typically found in fractions 4-7, as visually represented by the colored layers in the middle tube. (B) Further Purification and Characterization of Small EVs: This section details the subsequent purification steps. The fractions identified as containing small EVs (fractions 4-7) are collected and subjected to a wash step with PBS (120,000 x g, 1.5 hours, 4°C) to remove residual iodixanol or low-density pool fractions and contaminants. This washing step results in a purified "small EV pellet (25-500nm diameter)," as shown in the clear tube on the right. The purity and concentration of the isolated S.EVs are then confirmed: density confirmation is performed by measuring absorbance at 230nm of iodixanol across fractions, and protein concentration is determined using a Bradford assay. This comprehensive workflow ensures the isolation of a highly purified small EV population for downstream analysis.

4.4.Nano FCM and SYTOX Green staining.

Recent advancement in Flow Cytometry (FC) has allowed for EV analysis and involves the implementation of nanoscale FC (nFC, nanoFACS). This upgrade of conventional flow cytometry includes special enhancements in optical and fluidic systems, which allows for more accurate and

targeted analysis of EVs (Kowkabany & Bao, 2024).NanoFACS, a high-resolution flow cytometric method that utilizes light scattering and fluorescence parameters along with sample enumeration, to evaluate various labels. SYTO green (SYTOX) optimisation was determined by carrying out multiple dye concentrations in the range from 10 nM to 1 µM. Following this we added 1µl of 1µM solution to 2µl of each C.EVs and S.EVs at both air and physoxia. Samples were incubated for 1hr at room temperature. NanoFCM was performed with 10 µl of diluted EV samples (1:100) and analyzed using a Flow NanoAnalyzer fitted with a Blue Laser (488 nm) (NanoFCM, Inc.) for multiparameter analysis of EV samples, allowing quantitative analysis of single particles. All experiments were performed in compliance with the NanoFCM system's recommendations. Briefly, samples were individually tested to record a total number of 3,000-12,500 events. PBS was used for threshold setting and as blanks. Monodisperse silica nanoparticle cocktail (68-155 nm, Cat. S16M-Exo, NanoFCM, Inc.) and polystyrene (200 nm) beads at a 1/100 dilution (QC Beads, Cat. S08210, NanoFCM, Inc.) were used as size and particle concentration reference, respectively. Standard beads and all samples were collected under the same sampling pressure (1 kPa) for 1 min. Light scattering was applied for the measurement of nanoparticle size and size distributions. The EV size range was set between 40-300 nm. Fluorescence analyses were based on FITC-A. All applicable assay controls described by MIFLowCyt-EV guidelines (i.e. buffer controls, unstained samples or detergent treatment of stained samples) were evaluated. Data analysis was performed with the Nano FCM software NF Profession version 1.15/1.17.(Liu et al., 2022)

4.5. TNC EV Surface marker labelling

Crude and small EV samples from air oxygen and physoxia were analyzed using flow cytometry and the MACSPlex Exosome surface marker characterization kit (Miltenyi Biotec) for detection of the presence of 37 surface markers (CD1c, CD2, CD3, CD4, CD8, CD9, CD11c, CD14, CD19, CD20, CD24, CD25, CD29, CD31, CD40, CD41b, CD42a, CD44, CD45, CD49e, CD56, CD62p, CD63, CD69, CD81, CD86, CD105, CD133.1, CD142, CD146, CD209, CD326, HLA-ABC, HLA-DR DP DQ, MCSP, ROR1 and SSEA-4). This Kit uses the capture beads (4.8-µm diameter polystyrene beads, labelled with different amounts of 2 dyes phycoerythrin and fluorescein isothiocyanate), to generate 39 different bead subsets identifiable by flow cytometry analysis. Each bead subset is conjugated with a different capture anti-body that recognizes EVs carrying the respective antigen (37 EV surface epitopes plus 2 isotype controls). The list of 37 antigens and their respective biological functions are reported in supplementary materials (Table 1). EVs bound to beads are detected by allophycocyanin-conjugated anti-CD9, anti- CD63, and anti-CD81 antibodies (figure 10B). For each sample EV subgroup and respective controls (un-supplemented DMEM and blank control of MACS Plex Buffer), 200µl of EV samples containing 50 µg of total protein were diluted with 120 µl with of MACS Plex buffer, followed by the addition of 15 µl of capture bead solution to a total volume of 335 µl before an incubation at 4 °C under gentle agitation, overnight.

4.6.Flow cytometric data analysis and calculation of relative qualification of EV surface markers

The data analysis consists of the following steps: Background subtraction, data normalization (Calculation of normalization factor and normalization of detected signals) the signals for the tetraspanin markers CD9, CD63, and CD81 enable comparison of each profile by adapting the different signal ranges (steps 3–4). Calibration of the MACSQuant Analyzer using MACSQuant Calibration Beads (# 130-093-607) was ran following the manufacture's guidelines, EV samples (60 µL) diluted 1:2 in buffer solution were analysed with the MACS Quant Analyzer-10 flow cytometer (Miltenyi), initially the blank control (MACs plex buffer) was run to obtain the background signal. The 39 bead populations can be distinguished by different fluorescence intensities detected in the FITC and PE channel (B1 and B2 channel of MACSQuant Analyser's). Determination of relative EV surface marker levels: Background subtraction; The median signal intensity of each bead obtained from the control sample (buffer only) from the signal intensities of the respective beads incubated with the sample and was repeated for all samples to be analysed. Calculation of normalization factor: for each sample calculate the median signal intensity of the signals detected for the MACSPlex EV IO

Capture Beads CD9, CD63, and CD81.Normalization of detected signals: Divide the signal intensities of all beads by the normalization factor of the respective sample. The mean of the MACSPlex EV IO Capture Beads is thereby set to 1 or 100%. Determine the relative EV marker level by calculating the ratio of the signal intensities of each of the two samples to be compared.

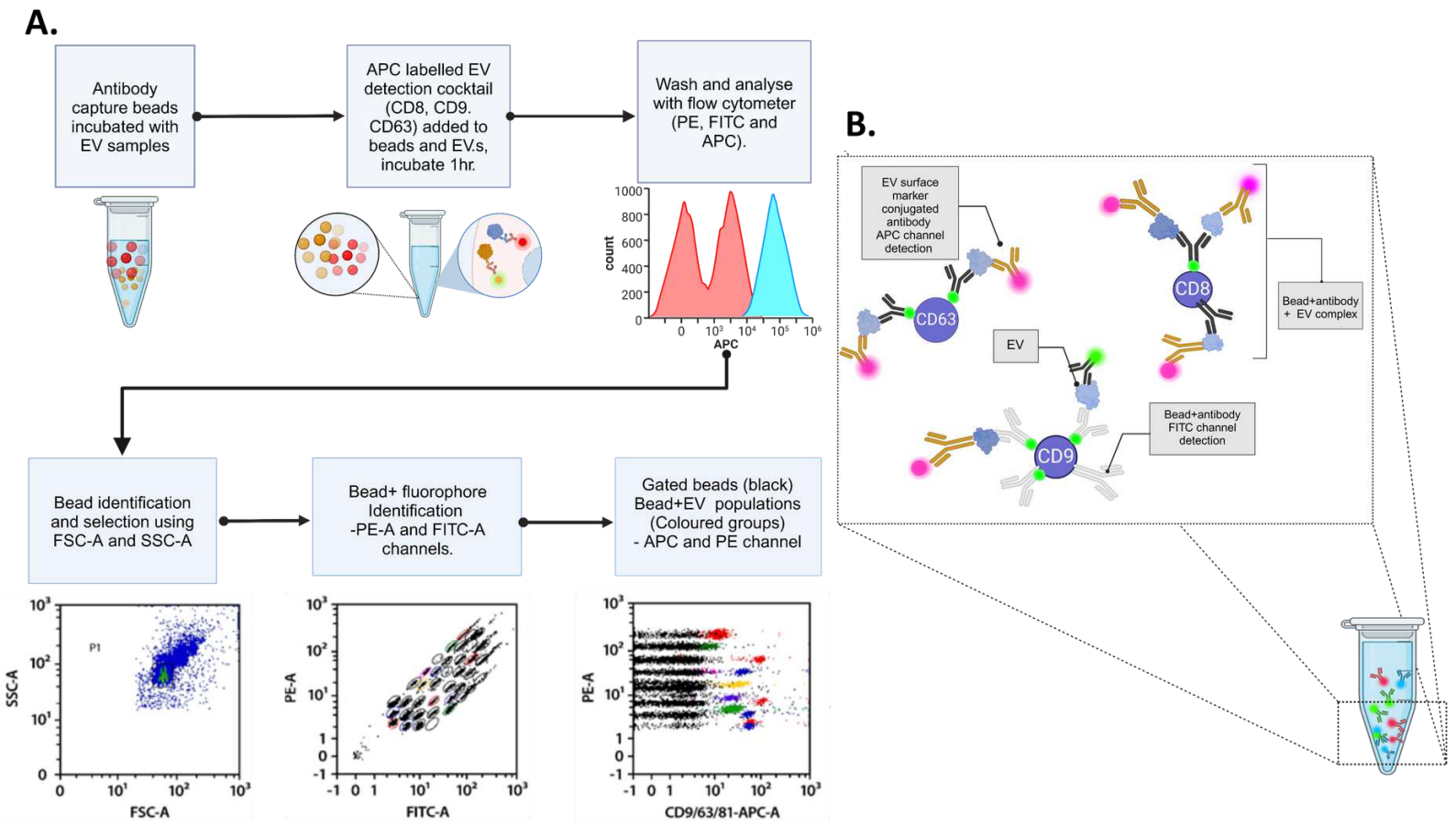


Figure 13. Flow Cytometry-Based Analysis of Extracellular Vesicle (EV) Surface Markers.(A) Workflow for EV Immunocapture and Flow Cytometric Detection: This flowchart details the experimental procedure for characterizing EV surface markers using antibody-conjugated beads and flow cytometry. First, antibody capture beads are incubated with EV samples in a tube. Subsequently, an APC (Allophycocyanin)-labeled EV detection cocktail containing antibodies against CD8, CD9, and CD63 is added and incubated for 1 hour. After incubation, the bead-EV complexes are washed and analyzed using a flow cytometer to detect PE (Phycoerythrin), FITC (Fluorescein Isothiocyanate), and APC fluorescence. The workflow then proceeds to bead identification and selection using forward scatter (FSC-A) and side scatter (SSC-A) plots. Following bead identification, fluorophore identification is performed using PE-A and FITC-A channels. Finally, gated beads are analyzed for Bead+EV populations, with different populations identified by their APC and PE channel fluorescence, allowing for multicolor detection of specific EV surface markers. The example histogram shows APC channel detection with peaks indicating different levels of marker expression or bead populations.(B) Schematic Representation of Bead-EV Immunocapture and Detection: This magnified schematic illustrates the molecular mechanism of EV capture and fluorescent detection. It shows an EV (represented as a grey sphere) complexed with magnetic or capture beads via specific antibodies (e.g., anti-CD63, anti-CD9). Fluorescently labeled detection antibodies (e.g., anti-CD8, anti-CD63, anti-CD9 conjugated with PE, FITC, or APC) then bind to specific surface markers on the captured EVs. This forms a bead-antibody-EV complex, which is subsequently detected by the flow cytometer based on the presence of the fluorophores, enabling the quantification and phenotyping of EV populations based on their surface protein expression.(Vacchi et al., 2020)

4.7.*Evaluation of cytokine content.*

The cytokine content of the TNC EV samples was determined using Eve technologies **Porcine Cytokine/Chemokine Panel** kit- GM-CSF, IFNy, IL-1a, IL-1b, IL-1ra, IL-2, IL-4, IL-6, IL-8, IL-10, IL-12, IL-18, TNF. Three technical replicate values were obtained for triplicate biological samples.

(*Discovery Assays - Eve Technologies*, n.d.) (Custom Plex Biomarkers - Eve Technologies, https://www.evetechnologies.com/discovery-assays-). The multiplexing technology used for this analysis, provided by Eve Technologies, is based on color-coded polystyrene beads. Bead coloration is achieved by using different concentrations of red and infrared fluorophore dyes to create 100 uniquely colored bead sets. Considering that these bead sets have a unique color/fluorophore signature (that can be individually identified by the bead analyzer (Bio-Plex200). In addition to our Multiplexing LASER Bead Technology, electrochemiluminescence(ECH). ECH allows for high sensitivity and precision.Sample volume; each sample subgroup was aliquoted in triplicate containing a protein concentration of 10µg/ml, for analysis in triplicate 750µl of conditioned media. Inter-assay variability ranges between 5-20% with this method. The standard curve is run following the kit manufacturer's instructions for use for each sample.

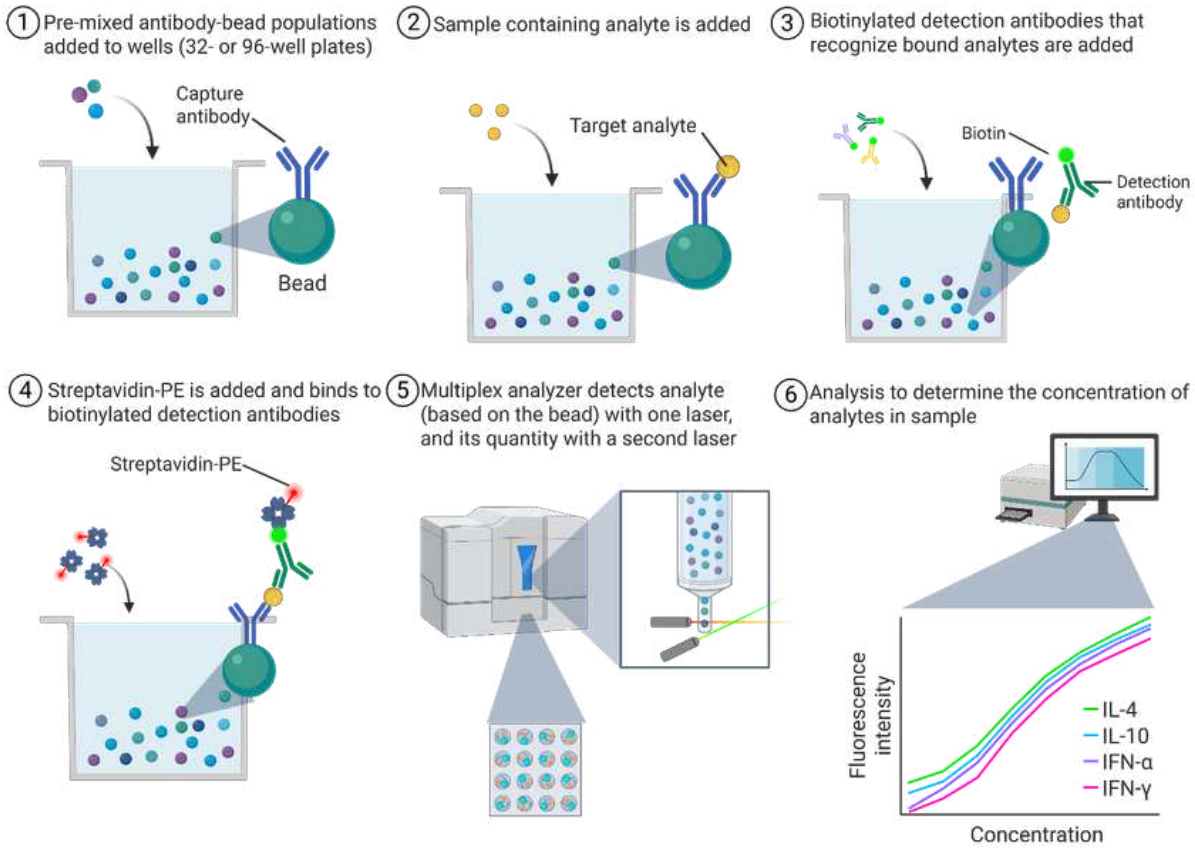


Figure 14. Quantiative Cytokine detection: Overview of capture bead detection methood and subsequent data quizisitio (https://www.evetechnologies.com/discovery-assays). This schematic outlines the sequential steps of a typical multiplex bead-based immunoassay, often used for simultaneous quantification of multiple analytes like cytokines in a single sample.(1) Pre-mixed Antibody-Bead Populations: The assay begins by adding pre-mixed populations of spectrally distinct beads (each encoded to represent a specific analyte) into wells of a 32- or 96-well plate. Each bead type is conjugated with a specific capture antibody designed to bind a particular target analyte.(2) Sample Containing Analyte is Added: The sample, containing the target analytes (e.g., cytokines) of interest, is then added to the wells. The analytes present in the sample bind specifically to their corresponding capture antibodies on the beads.(3) Biotinylated Detection Antibodies are Added: Following incubation and washing steps, biotinylated detection antibodies, which are specific to different epitopes of the bound analytes, are added. These detection antibodies bind to the captured analytes, forming a "sandwich" complex on the beads.(4) Streptavidin-PE is Added: Streptavidin, conjugated with a fluorescent reporter molecule like Phycoerythrin (PE), is then added. Streptavidin has a high affinity for biotin and binds to the biotinylated detection antibodies, effectively labeling the entire immunocomplex with a fluorescent signal.(5) Multiplex Analyzer Detection: The beads are then analyzed using a multiplex analyzer (e.g., Luminex platform). This instrument uses two lasers: one laser identifies the unique spectral signature of each bead population (identifying the analyte), and a second laser quantifies the fluorescence intensity of the PE reporter molecule on each bead (measuring the amount of bound analyte).(6) Analysis and Quantification: The raw fluorescence intensity data for each bead type is then analyzed to determine the concentration of each specific analyte in the original sample. A standard curve (represented by the graph showing fluorescence intensity versus

concentration for different analytes like IL-4, IL-10, IFN-α, IFN-γ) is generated using known concentrations of purified analytes, allowing for accurate quantification of unknown samples.

5. Statistical analysis.

Data are presented as means ▯SD. For normally distributed data, differences between groups were tested using a one-way ANOVA followed by Bonferroni post hoc sorting. Data that was not normally distributed was tested using a Kruskal-Wallis test followed by Dunn's multiple comparisons test. Statistical analyses were conducted using Prism software (version 8.0, GraphPad, La Jolla, CA).Differences were considered statistically significant when $P<0.05$.

8. Refrences

Amraei, R., Yin, W., Napoleon, M. A., Suder, E. L., Berrigan, J., Zhao, Q., Olejnik, J., Chandler, K. B., Xia, C., Feldman, J., Hauser, B. M., Caradonna, T. M., Schmidt, A. G., Gummuluru, S., Muhlberger, E., Chitalia, V., Costello, C. E., & Rahimi, N. (2020). CD209L/L-SIGN and CD209/DC-SIGN act as receptors for SARS-CoV-2 and are differentially expressed in lung and kidney epithelial and endothelial cells. BioRxiv. https://doi.org/10.1101/2020.06.22.165803

Arvind, V., Crosio, G., Howell, K., Zhang, H., Montero, A., & Huang, A. H. (2025). Functional tendon regeneration is driven by regulatory T cells and IL-33 signaling. Science Advances , 11(17). https://doi.org/10.1126/SCIADV.ADN5409/SUPPL_FILE/SCIADV.ADN5409_DATA_S1_AND_S2.ZIP

Baksh, D., Zandstra, P. W., & Davies, J. E. (2007). A non-contact suspension culture approach to the culture of osteogenic cells derived from a CD49elow subpopulation of human bone marrow-derived cells. Biotechnology and Bioengineering, 98(6), 1195–1208. https://doi.org/10.1002/BIT.21556;WGROUP:STRING:PUBLICATION

Barboni, B., Curini, V., Russo, V., Mauro, A., Giacinto, O., Marchisio, M., Alfonsi, M., & Mattioli, M. (2012). Indirect co-culture with tendons or tenocytes can program amniotic epithelial cells towards stepwise tenogenic differentiation. PLoS ONE, 7(2). https://doi.org/10.1371/JOURNAL.PONE.0030974

Barboni, B., Russo, V., Gatta, V., Bernabò, N., Berardinelli, P., Mauro, A., Martelli, A., Valbonetti, L., Muttini, A., Di Giacinto, O., Turriani, M., Silini, A., Calabrese, G., Abate, M., Parolini, O., Stuppia, L., & Mattioli, M. (2018). Therapeutic potential of hAECs for early Achilles tendon defect repair through regeneration. Journal of Tissue Engineering and Regenerative Medicine, 12(3), e1594–e1608. https://doi.org/10.1002/TERM.2584;PAGEGROUP:STRING:PUBLICATION

Binnewies, M., Mujal, A. M., Pollack, J. L., Combes, A. J., Hardison, E. A., Barry, K. C., Tsui, J., Ruhland, M. K., Kersten, K., Abushawish, M. A., Spasic, M., Giurintano, J. P., Chan, V., Daud, A. I., Ha, P., Ye, C. J., Roberts, E. W., & Krummel, M. F. (2019). Unleashing Type-2 Dendritic Cells to Drive Protective Antitumor CD4+ T Cell Immunity. Cell, 177(3), 556-571.e16. https://doi.org/10.1016/J.CELL.2019.02.005/ATTACHMENT/4201B17C-C51B-4409-A280-2ED4F52D4F40/MMC4.XLSX

Boussiotis, V. A., Freeman, G. J., Griffin, J. D., Gray, G. S., Gribben, J. G., & Nadler, L. M. (1994). CD2 is involved in maintenance and reversal of human alloantigen-specific clonal anergy. Journal of Experimental Medicine, 180(5), 1665–1673. https://doi.org/10.1084/JEM.180.5.1665

Buckley, C. D., Simón-Campos, J. A., Zhdan, V., Becker, B., Davy, K., Fisheleva, E., Gupta, A., Hawkes, C., Inman, D., Layton, M., Mitchell, N., Patel, J., Saurigny, D., Williamson, R., & Tak, P. P. (2020). Efficacy, patient-reported outcomes, and safety of the anti-granulocyte macrophage colony-stimulating factor antibody otilimab (GSK3196165) in patients with rheumatoid arthritis: a

randomised, phase 2b, dose-ranging study. The Lancet Rheumatology, 2(11), e677–e688. https://doi.org/10.1016/S2665-9913(20)30229-0

Buckley, C., Simón-Campos, J., Zhdan, V., & al., et. (2020). Efficacy, patient-reported outcomes, and safety of the anti-granulocyte macrophage colony-stimulating factor antibody otilimab (GSK3196165) in patients with rheumatoid arthritis: a randomised, phase 2b, dose-ranging study. Lancet Rheumatol.

Bullough, R., Finnigan, T., Kay, A., Maffulli, N., & Forsyth, N. R. (2008). Tendon repair through stem cell intervention: Cellular and molecular approaches. Disability and Rehabilitation, 30(20–22), 1746–1751. https://doi.org/10.1080/09638280701788258

Bykerk, V. P. (2020). The efficacy and safety of targeting GM-CSF in arthritis. The Lancet Rheumatology, 2(11), e648–e650. https://doi.org/10.1016/S2665-9913(20)30352-0

Canosa-Carro, L., Bravo-Aguilar, M., Abuín-Porras, V., Almazán-Polo, J., García-Pérez-de-Sevilla, G., Rodríguez-Costa, I., López-López, D., Navarro-Flores, E., & Romero-Morales, C. (2022). Current understanding of the diagnosis and management of the tendinopathy: An update from the lab to the clinical practice. Disease-a-Month, 68(10), 101314. https://doi.org/10.1016/J.DISAMONTH.2021.101314

Chen, L., Liu, J.-P., Tang, K.-L., Wang, Q., Wang, G.-D., Cai, X.-H., & Liu, X.-M. (2014). Tendon Derived Stem Cells Promote Platelet-Rich Plasma Healing in Collagenase-Induced Rat Achilles Tendinopathy. Cellular Physiology and Biochemistry, 34(6), 2153–2168. https://doi.org/10.1159/000369659

Chen, Z., Chen, P., Zheng, M., Gao, J., Liu, D., Wang, A., Zheng, Q., Leys, T., Tai, A., & Zheng, M. (2022). Challenges and perspectives of tendon-derived cell therapy for tendinopathy: from bench to bedside. Stem Cell Research and Therapy, 13(1). https://doi.org/10.1186/s13287-022-03113-6

Chiron, S., Tomczak, C., Duperray, A., Lainé, J., Bonne, G., Eder, A., Hansen, A., Eschenhagen, T., Verdier, C., & Coirault, C. (2012). Complex Interactions between Human Myoblasts and the Surrounding 3D Fibrin-Based Matrix. PLoS ONE, 7(4), e36173. https://doi.org/10.1371/journal.pone.0036173

Chua, J. S., Chng, C. P., Moe, A. A. K., Tann, J. Y., Goh, E. L. K., Chiam, K. H., & Yim, E. K. F. (2014). Extending neurites sense the depth of the underlying topography during neuronal differentiation and contact guidance. Biomaterials, 35(27), 7750–7761. https://doi.org/10.1016/J.BIOMATERIALS.2014.06.008

Clerici, M., Citro, V., Byrne, A. L., Dale, T. P., Boccaccini, A. R., Della Porta, G., Maffulli, N., & Forsyth, N. R. (2023). Endotenon-Derived Type II Tendon Stem Cells Have Enhanced Proliferative and Tenogenic Potential. International Journal of Molecular Sciences, 24(20). https://doi.org/10.3390/ijms242015107

Correction to "Minimal information for studies of extracellular vesicles (MISEV2023): From basic to advanced approaches"(Journal of Extracellular Vesicles, (2024), 13, (e12404), 10.1002/jev2.12404). (2024). Journal of Extracellular Vesicles, 13(5). https://doi.org/10.1002/JEV2.12451

Crescitelli, R., Lässer, C., & Lötvall, J. (2021). Isolation and characterization of extracellular vesicle subpopulations from tissues. Nature Protocols 2021 16:3, 16(3), 1548–1580. https://doi.org/10.1038/s41596-020-00466-1

Custom Plex Biomarkers - Eve Technologies. (n.d.). Retrieved June 28, 2025, from https://www.evetechnologies.com/custom-plex-biomarkers/?cat=porcine

Daigneault, M., Preston, J. A., Marriott, H. M., Whyte, M. K. B., & Dockrell, D. H. (2010). The Identification of Markers of Macrophage Differentiation in PMA-Stimulated THP-1 Cells and Monocyte-Derived Macrophages. PLOS ONE, 5(1), e8668. https://doi.org/10.1371/JOURNAL.PONE.0008668

Digital Surf - Surface Imaging, Analysis and Metrology Software. (n.d.). Retrieved October 25, 2024, from https://www.digitalsurf.com/

Discovery Assays - Eve Technologies. (n.d.). Retrieved June 28, 2025, from https://www.evetechnologies.com/discovery-assays-2/

Domnick, C., Wieskötter, B., Raschke, M. J., Schulze, M., Kronenberg, D., Wefelmeier, M., Langer, M. F., & Herbort, M. (2016). Evaluation of biomechanical properties: are porcine flexor tendons and bovine extensor tendons eligible surrogates for human tendons in in vitro studies? Archives of Orthopaedic and Trauma Surgery, 136(10), 1465–1471. https://doi.org/10.1007/S00402-016-2529-2

Doyle, L. M., & Wang, M. Z. (2019). Overview of extracellular vesicles, their origin, composition, purpose, and methods for exosome isolation and analysis. Cells, 8(7), 727. https://doi.org/10.3390/cells8070727

Duffield, A., Kamsteeg, E. J., Brown, A. N., Pagel, P., & Caplan, M. J. (2003). The tetraspanin CD63 enhances the internalization of the H,K-ATPase β-subunit. Proceedings of the National Academy of Sciences of the United States of America, 100(26), 15560–15565. https://doi.org/10.1073/PNAS.2536699100/ASSET/F288E053-49B8-43A5-AD33-165FC62E540D/ASSETS/GRAPHIC/ZPQ0250366990007.JPEG

Fan, C., Zhao, Y., Chen, Y., Qin, T., Lin, J., Han, S., Yan, R., Lei, T., Xie, Y., Wang, T., Gu, S., Ouyang, H., Shen, W., Yin, Z., & Chen, X. (2022). A Cd9+Cd271+ stem/progenitor population and the SHP2 pathway contribute to neonatal-to-adult switching that regulates tendon maturation. Cell Reports, 39(4). https://doi.org/10.1016/j.celrep.2022.110762

Garcia-Melchor, E., Cafaro, G., MacDonald, L., Crowe, L. A. N., Sood, S., McLean, M., Fazzi, U. G., McInnes, I. B., Akbar, M., & Millar, N. L. (2021). Novel self-amplificatory loop between T cells and tenocytes as a driver of chronicity in tendon disease. Annals of the Rheumatic Diseases, 80(8), 1075. https://doi.org/10.1136/ANNRHEUMDIS-2020-219335

Genovese, M. C., Berkowitz, M., Conaghan, P. G., Peterfy, C., Davy, K., Fisheleva, E., Gupta, A., Inman, D., Janiczek, R., Layton, M., Mitchell, N., Patel, J., Roberts, A., Saurigny, D., Smith, J. E., Williamson, R., & Tak, P. P. (2020). MRI of the joint and evaluation of the granulocyte–macrophage colony-stimulating factor–CCL17 axis in patients with rheumatoid arthritis receiving otilimab: a phase 2a randomised mechanistic study. The Lancet Rheumatology, 2(11), e666–e676. https://doi.org/10.1016/S2665-9913(20)30224-1

Graça, A. L., Domingues, R. M. A., Gomez-Florit, M., & Gomes, M. E. (2023). Platelet-Derived Extracellular Vesicles Promote Tenogenic Differentiation of Stem Cells on Bioengineered Living Fibers. International Journal of Molecular Sciences, 24(4). https://doi.org/10.3390/IJMS24043516

High throughput assessment of platelet signaling, function and inhibition. (n.d.). https://doi.org/10.26481/dis.20230623df

Iwai, K., Yamamoto, S., Yoshida, M., & Shiba, K. (2017). Isolation of Extracellular Vesicles in Saliva Using Density Gradient Ultracentrifugation. Methods in Molecular Biology (Clifton, N.J.), 1660, 343–350. https://doi.org/10.1007/978-1-4939-7253-1_27

Jones, E. R., Jones, G. C., Legerlotz, K., & Riley, G. P. (2013). Cyclical strain modulates metalloprotease and matrix gene expression in human tenocytes via activation of TGFβ. Biochimica et Biophysica Acta (BBA) - Molecular Cell Research, 1833(12), 2596–2607. https://doi.org/10.1016/j.bbamcr.2013.06.019

Kamizaki, K., Doi, R., Hayashi, M., Saji, T., Kanagawa, M., Toda, T., Fukada, S. ichiro, Ho, H. Y. H., Greenberg, M. E., Endo, M., & Minami, Y. (2017). The Ror1 receptor tyrosine kinase plays a critical role in regulating satellite cell proliferation during regeneration of injured muscle. The Journal of Biological Chemistry, 292(38), 15939. https://doi.org/10.1074/JBC.M117.785709

Kappelmayer, J., & Nagy, B. (2017). The Interaction of Selectins and PSGL-1 as a Key Component in Thrombus Formation and Cancer Progression. BioMed Research International, 2017(1), 6138145. https://doi.org/10.1155/2017/6138145

Kasula, V., Padala, V., Gupta, N., Doyle, D., Bagheri, K., Anastasio, A., & Adams, S. B. (2024). The Use of Extracellular Vesicles in Achilles Tendon Repair: A Systematic Review. Biomedicines, 12(5), 942. https://doi.org/10.3390/BIOMEDICINES12050942/S1

Kay, A. G., Dale, T. P., Akram, K. M., Mohan, P., Hampson, K., Maffulli, N., Spiteri, M. A., El Haj, A. J., & Forsyth, N. R. (2015). BMP2 Repression and Optimized Culture Conditions Promote Human Bone Marrow-Derived Mesenchymal Stem Cell Isolation. Regenerative Medicine, 10(2), 109–125. https://doi.org/10.2217/RME.14.67

Kay, A. G., Long, G., Tyler, G., Stefan, A., Broadfoot, S. J., Piccinini, A. M., Middleton, J., & Kehoe, O. (2017). Mesenchymal Stem Cell-Conditioned Medium Reduces Disease Severity and Immune Responses in Inflammatory Arthritis. Scientific Reports 2017 7:1, 7(1), 1–11. https://doi.org/10.1038/s41598-017-18144-w

Khan, K. M., Cook, J. L., Bonar, F., Harcourt, P., & Åstrom, M. (1999). Histopathology of common tendinopathies. Update and implications for clinical management. Sports Med., 27(6), 393–408. https://doi.org/10.2165/00007256-199927060-00004

Klatte-Schulz, F., Gehlen, T., Bormann, N., Tsitsilonis, S., Manegold, S., Schmock, A., Melzer, J. A., Schmidt-Bleek, K., Geißler, S., Duda, G. N., Sawitzki, B., & Wildemann, B. (2024). INCREASED CD4+ TO CD8+ T-CELL RATIO AS A DRIVER OF IMPAIRED ACHILLES TENDON HEALING IN HUMAN PATIENTS. Orthopaedic Proceedings, 106-B(SUPP_2), 29–29. https://doi.org/10.1302/1358-992X.2024.2.029

Koliha, N., Heider, U., Bosio, A., & Wild, S. (2015). Normalized signal intensities of different capture antibody beads after overnight incubation with 64 µg of plasma exosomes from four donors (D1-D4) and staining with a cocktail of CD9-APC, CD63-APC, and CD81-APC antibodies for 1 h. A multiplex bead platform for the characterization of cell culture-and plasma-derived exosomes. https://static.miltenyibiotec.com/asset/150655405641/document_f09qqs30pt58b227m03rqmsi0c?content-disposition=inline

Kowkabany, G., & Bao, Y. (2024). Nanoparticle Tracking Analysis: An Effective Tool to Characterize Extracellular Vesicles. Molecules (Basel, Switzerland), 29(19). https://doi.org/10.3390/molecules29194672

Kragsnaes, M. S., Fredberg, U., Stribolt, K., Kjaer, S. G., Bendix, K., & Ellingsen, T. (2014). Stereological quantification of immune-competent cells in baseline biopsy specimens from achilles tendons: Results from patients with chronic tendinopathy followed for more than 4 years. American Journal of Sports Medicine, 42(10), 2435–2445. https://doi.org/10.1177/0363546514542329

Lancaster, S. T., & Mahadevan, D. (2021). Current concepts review: Management of Achilles tendinopathy overview. Journal of Arthroscopy and Joint Surgery, 8(3), 216–221. https://doi.org/10.1016/j.jajs.2021.03.002

Lee, J., Smeriglio, P., Dragoo, J., Maloney, W. J., & Bhutani, N. (2016). CD24 enrichment protects while its loss increases susceptibility of juvenile chondrocytes towards inflammation. Arthritis Research and Therapy, 18(1), 1–11. https://doi.org/10.1186/S13075-016-1183-Y/FIGURES/6

Li, J., Chen, S., Li, Y., Zhu, Z., Huang, H., Wang, W., Yang, Y., Liang, Y., & Shu, L. (2022). Comprehensive Profiling Analysis of CD209 in Malignancies Reveals the Therapeutic Implication for Tumor Patients Infected With SARS-CoV-2. Frontiers in Genetics, 13, 883234. https://doi.org/10.3389/FGENE.2022.883234/BIBTEX

Liu, H., Tian, Y., Xue, C., Niu, Q., Chen, C., & Yan, X. (2022). Analysis of extracellular vesicle DNA at the single-vesicle level by nano-flow cytometry. J. Extracell. Vesicle, 11(4), e12206. https://doi.org/10.1002/jev2.12206

Loh, C. Y. Y., Wang, A. Y. L., Tiong, V. T. Y., Athanassopoulos, T., Loh, M., Lim, P., & Kao, H. K. (2018). Animal models in plastic and reconstructive surgery simulation—a review. Journal of Surgical Research, 221, 232–245. https://doi.org/10.1016/j.jss.2017.08.052

Lui, P. P. Y. (2015a). Markers for the identification of tendon-derived stem cells in vitro and tendon stem cells in situ - Update and future development. Stem Cell Research and Therapy, 6(1), 1–9. https://doi.org/10.1186/S13287-015-0097-Y/METRICS

Lui, P. P. Y. (2015b). Markers for the identification of tendon-derived stem cells in vitro and tendon stem cells in situ – update and future development. Stem Cell Research & Therapy, 6(1), 106. https://doi.org/10.1186/S13287-015-0097-Y

Lui, P. P. Y., Maffulli, N., Rolf, C., & Smith, R. K. W. (2011). What are the validated animal models for tendinopathy? Scand. J. Med. Sci. Sports, 21(1), 3–17. https://doi.org/10.1111/j.1600-0838.2010.01164.x

M Bottagisio, A. L. (2017). A review on animal models and treatments for the reconstruction of Achilles and flexor tendons. J. Mater. Sci. Mater. Med., 28, 45.

Marr, N., Meeson, R., Kelly, E. F., Fang, Y., Peffers, M. J., Pitsillides, A. A., Dudhia, J., & Thorpe, C. T. (2021). Cd146 delineates an interfascicular cell sub-population in tendon that is recruited during injury through its ligand laminin-α4. International Journal of Molecular Sciences, 22(18). https://doi.org/10.3390/IJMS22189729,

Marsolais, D., Côté, C. H., & Frenette, J. (2001). Neutrophils and macrophages accumulate sequentially following Achilles tendon injury. Journal of Orthopaedic Research, 19(6), 1203–1209. https://doi.org/10.1016/S0736-0266(01)00031-6

Mayassi, T., Barreiro, L. B., Rossjohn, J., & Jabri, B. (2021). A multilayered immune system through the lens of unconventional T cells. Nature 2021 595:7868, 595(7868), 501–510. https://doi.org/10.1038/s41586-021-03578-0

Meregalli, M., Farini, A., Belicchi, M., & Torrente, Y. (2010). CD133+ cells isolated from various sources and their role in future clinical perspectives. Expert Opinion on Biological Therapy, 10(11), 1521–1528. https://doi.org/10.1517/14712598.2010.528386,

Minami, Y., Oishi, I., Endo, M., & Nishita, M. (2010). Ror-family receptor tyrosine kinases in noncanonical Wnt signaling: Their implications in developmental morphogenesis and human diseases. Developmental Dynamics, 239(1), 1–15. https://doi.org/10.1002/DVDY.21991

Noah, A. C., Li, T. M., Martinez, L. M., Wada, S., Swanson, J. B., Disser, N. P., Sugg, K. B., Rodeo, S. A., Lu, T. T., & Mendias, C. L. (2020). Adaptive and innate immune cell responses in tendons and lymph nodes after tendon injury and repair. Journal of Applied Physiology, 128(3), 473. https://doi.org/10.1152/JAPPLPHYSIOL.00682.2019

Notti, R. Q., Yi, F., Heissel, S., Bush, M. W., Molvi, Z., Das, P., Molina, H., Klebanoff, C. A., & Walz, T. (2024). The resting state of the human T-cell receptor–CD3 complex. BioRxiv, 1, 2023.08.22.554360. https://doi.org/10.1101/2023.08.22.554360

Oreff, G. L., Fenu, M., Vogl, C., Ribitsch, I., & Jenner, F. (2021). Species variations in tenocytes' response to inflammation require careful selection of animal models for tendon research. Scientific Reports 2021 11:1, 11(1), 1–14. https://doi.org/10.1038/s41598-021-91914-9

Pauly, S., Klatte, F., Strobel, C., Schmidmaier, G., Greiner, S., Scheibel, M., & Wildemann, B. (2010). Characterization of tendon cell cultures of the human rotator cuff. European Cells and Materials, 20, 84–97. https://doi.org/10.22203/eCM.v020a08

Peterson, A., & Seed, B. (1987). Monoclonal antibody and ligand binding sites of the T cell erythrocyte receptor (CD2). Nature, 329(6142), 842–846. https://doi.org/10.1038/329842A0

Rieu, S., Géminard, C., Rabesandratana, H., Sainte-Marie, J., & Vidal, M. (2000). Exosomes released during reticulocyte maturation bind to fibronectin via integrin alpha4beta1. Eur. J. Biochem., 267(2), 583–590. https://doi.org/10.1046/j.1432-1327.2000.01036.x

Royo, F., Théry, C., Falcón-Pérez, J. M., Nieuwland, R., & Witwer, K. W. (2020). Methods for Separation and Characterization of Extracellular Vesicles: Results of a Worldwide Survey Performed by the ISEV Rigor and Standardization Subcommittee. Cells, 9(9). https://doi.org/10.3390/CELLS9091955

Russo, V., El Khatib, M., Prencipe, G., Citeroni, M. R., Faydaver, M., Mauro, A., Berardinelli, P., Cerveró-Varona, A., Haidar-Montes, A. A., Turriani, M., Di Giacinto, O., Raspa, M., Scavizzi, F., Bonaventura, F., Stöckl, J., & Barboni, B. (2022). Tendon Immune Regeneration: Insights on the Synergetic Role of Stem and Immune Cells during Tendon Regeneration. Cells, 11(3). https://doi.org/10.3390/CELLS11030434

Shih, Y.-R. V, Tseng, K.-F., Lai, H.-Y., Lin, C.-H., & Lee, O. K. (2011). Matrix stiffness regulation of integrin-mediated mechanotransduction during osteogenic differentiation of human mesenchymal stem cells. Journal of Bone and Mineral Research, 26(4), 730–738. https://doi.org/10.1002/jbmr.278

Stout, R., Jiang, C., Matta, B., Tietzel, I., & Watkins, S. (2005). Macrophages sequentially change their functional phenotype in response to changes in microenvironmental influences. J Immunol, 175.

Tsuzaki, M., Guyton, G., Garrett, W., Archambault, J. M., Herzog, W., Almekinders, L., Bynum, D., Yang, X., & Banes, A. J. (2003). IL-1 beta induces COX2, MMP-1, -3 and -13, ADAMTS-4, IL-1 beta and IL-6 in human tendon cells. J. Orthop. Res., 21(2), 256–264. https://doi.org/10.1016/s0736-0266(02)00141-9

Vacchi, E., Burrello, J., Di Silvestre, D., Burrello, A., Bolis, S., Mauri, P., Vassalli, G., Cereda, C. W., Farina, C., Barile, L., Kaelin-Lang, A., & Melli, G. (2020). Immune profiling of plasma-derived extracellular vesicles identifies Parkinson disease. Neurology(R) Neuroimmunology & Neuroinflammation, 7(6). https://doi.org/10.1212/NXI.0000000000000866

Van Deun, J., Mestdagh, P., Sormunen, R., Cocquyt, V., Vermaelen, K., Vandesompele, J., Bracke, M., De Wever, O., & Hendrix, A. (2014). The impact of disparate isolation methods for extracellular

vesicles on downstream RNA profiling. J. Extracell. Vesicles, 3(1), 24858. https://doi.org/10.3402/jev.v3.24858

Wang, H., Cheng, P., Wang, J., Lv, H., Han, J., Hou, Z., Xu, R., & Chen, W. (2025). Advances in spatial transcriptomics and its application in the musculoskeletal system. Bone Research 2025 13:1, 13(1), 1–21. https://doi.org/10.1038/s41413-025-00429-w

Wang, Y., He, G., Guo, Y., Tang, H., Shi, Y., Bian, X., Zhu, M., Kang, X., Zhou, M., Lyu, J., Yang, M., Mu, M., Lai, F., Lu, K., Chen, W., Zhou, B., Zhang, J., & Tang, K. (2019a). Exosomes from tendon stem cells promote injury tendon healing through balancing synthesis and degradation of the tendon extracellular matrix. Journal of Cellular and Molecular Medicine, 23(8), 5475. https://doi.org/10.1111/JCMM.14430

Wang, Y., He, G., Guo, Y., Tang, H., Shi, Y., Bian, X., Zhu, M., Kang, X., Zhou, M., Lyu, J., Yang, M., Mu, M., Lai, F., Lu, K., Chen, W., Zhou, B., Zhang, J., & Tang, K. (2019b). Exosomes from tendon stem cells promote injury tendon healing through balancing synthesis and degradation of the tendon extracellular matrix. Journal of Cellular and Molecular Medicine, 23(8), jcmm.14430. https://doi.org/10.1111/jcmm.14430

Wellings, E. P., Huang, T. C. T., Li, J., Peterson, T. E., Hooke, A. W., Rosenbaum, A., Zhao, C. D., Behfar, A., Moran, S. L., & Houdek, M. T. (2021). Intrinsic Tendon Regeneration After Application of Purified Exosome Product: An In Vivo Study. Orthopaedic Journal of Sports Medicine, 9(12). https://doi.org/10.1177/23259671211062929/ASSET/IMAGES/LARGE/10.1177_23259671211062929-FIG8.JPEG

Welsh, J. A., Goberdhan, D. C. I., O'Driscoll, L., Buzas, E. I., Blenkiron, C., Bussolati, B., Cai, H., Di Vizio, D., Driedonks, T. A. P., Erdbrügger, U., Falcon-Perez, J. M., Fu, Q. L., Hill, A. F., Lenassi, M., Lim, S. K., Mahoney, M. ỹ. G., Mohanty, S., Möller, A., Nieuwland, R., … Zubair, H. (2024). Minimal information for studies of extracellular vesicles (MISEV2023): From basic to advanced approaches. Journal of Extracellular Vesicles, 13(2), e12404. https://doi.org/10.1002/JEV2.12404

Witwer, K. W., Goberdhan, D. C. I., O'Driscoll, L., Théry, C., Welsh, J. A., Blenkiron, C., Buzás, E. I., Di Vizio, D., Erdbrügger, U., Falcón-Pérez, J. M., Fu, Q. L., Hill, A. F., Lenassi, M., Lötvall, J., Nieuwland, R., Ochiya, T., Rome, S., Sahoo, S., & Zheng, L. (2021). Updating MISEV: Evolving the minimal requirements for studies of extracellular vesicles. Journal of Extracellular Vesicles, 10(14). https://doi.org/10.1002/jev2.12182

Wu, J., Weisshaar, N., Weisshaar, N., Hotz-Wagenblatt, A., Madi, A., Madi, A., Ma, S., Mieg, A., Mieg, A., Hering, M., Mohr, K., Schlimbach, T., Borgers, H., Cui, G., & Cui, G. (2020). Skeletal muscle antagonizes antiviral CD8+ T cell exhaustion. Science Advances, 6(24), eaba3458. https://doi.org/10.1126/SCIADV.ABA3458

Xue, Z., Chen, Z., Wu, T., Li, R., Chen, C., Liu, J., Hou, H., Zheng, X., & Wang, H. (2022). VEGFA-Enriched Exosomes from Tendon-Derived Stem Cells Facilitate Tenocyte Differentiation, Migration, and Transition to a Fibroblastic Phenotype. BioMed Research International, 2022(1), 8537959. https://doi.org/10.1155/2022/8537959

Zhou, R., Tardivel, A., Thorens, B., Choi, I., & Tschopp, J. (2010). Thioredoxin-interacting protein links oxidative stress to inflammasome activation. Nature Immunology, 11(2), 136–140. https://doi.org/10.1038/ni.1831

6. Supplementary information.

Table 1. EV nomenclature stated by ISEV and referenced within this publication.(Witwer et al., 2021)

Term	Definition	Usage	
Extracellular vesicles (EVs)	Particles that are released from cells, are delimited by a lipid bilayer, and cannot replicate on their own.	Recommended	
Non-vesicular extracellular particles (NVEPs)	Multimolecular assemblies that are released from cells and do not have a lipid bilayer (non-vesicular extracellular particle fraction).	Recommended	
Extracellular particles (EPs)	Umbrella term for all particles outside the cell, including EVs and NVEPs.	Recommended	
EV mimetic	EV-like particles that are produced through direct artificial manipulation. This term is preferred over 'exosome-like vesicles' and similar terms that imply specific biogenesis-related properties.	Recommended	
Artificial cell-derived vesicles (ACDVs)	EV mimetics that are produced in the laboratory under conditions of induced cell disruption, such as extrusion.	Recommended	
Synthetic vesicles (SVs)	EV mimetics that are synthesized de novo from molecular components or made as hybrid entities, e.g., fusions between liposomes and native EVs.	Recommended	
Small EVs (operational term)	Based on the diameter of the separated particles, small EVs are often described as <200 nm in diameter. However, measured diameter is related to the specific characterization method.	Recommended, but caution required	
Large EVs (operational term)	Based on the diameter of the separated particles, large EVs are often described as >200 nm in diameter. However, measured diameter is related to the specific characterization method.	Recommended, but caution required	
Other 'operational terms'	Physical characteristics: e.g., diameter: small extracellular vesicles (sEVs), large EVs (lEVs), density: low, medium, high (defined ranges). Biochemical composition: e.g., contains a specific (macro)molecule, such as a protein. Cellular origin and/or conditions under which EVs were generated: terms that highlight specific aspects of biogenesis such as molecular mechanisms, energy-dependence (or lack thereof) and functional state of the parent cell related to stress or death.	Recommended, but caution required	

Exosome	Biogenesis-related term indicating origin from the endosomal system. Unless subcellular origin can be demonstrated, it is likely that a broad population of EVs is being studied, not exosomes specifically. Exosomes represent a subtype of small EVs: the diameter of intraluminal vesicles of endosomes is generally smaller than 200 nm.	Discouraged unless subcellular origin can be demonstrated
Ectosome	Biogenesis-related term indicating origin from the plasma membrane. Unless subcellular origin can be demonstrated it is likely that a broad population of EVs is being studied, not ectosomes specifically. Ectosomes can have a wide range of sizes, including sizes similar to those of exosomes.	Discouraged unless subcellular origin can be demonstrated
Microvesicle	Biogenesis-related term indicating origin from the plasma membrane. However, historically, the term has often been used to designate large EVs or all EVs, whatever their subcellular origin. This term can therefore lead to confusion.	Discouraged
Exosome-like vesicles	As 'exosome' is a biogenesis-related term indicating origin from the endosomal system, this and similar terms are discouraged for synthesized EV mimetics.	Discouraged

Table : Descriptions and biological roles of the markers tested using the MACS plex EV surface marker kit (Koliha et al., 2015).

EV-surface marker description		Role	Refrence
CD1c	APC cells surface glycoprotein	Antigen-presenting protein, **marker for dendritic cell subsets**	(Binnewies et al., 2019; Mayassi et al., 2021)
CD2	T and NK cell surface antigen	Mediator of adhesion between T-cells and other cell types	(Boussiotis et al., 1994; Peterson & Seed, 1987)
CD3	T cells surface glycoprotein	Mediator of signal transduction, CD3 is initially expressed in the cytoplasm of pro-thymocytes, the stem cells from which T-cells arise in the thymus.	(Notti et al., 2024)
CD4	T cells transmembrane glycoprotein	Co-receptor for MHC class II molecule, involved in the adaptive immune response to tendon injury	(Marsolais et al., 2001; Noah et al., 2020)
CD8	T cells transmembrane glycoprotein	Co-receptor for MHC class I molecule, /CD8+ T-cell ratio prognostic marker for early identification of patients with impaired tendon healing.	(Klatte-Schulz et al., 2024; Wu et al., 2020)
CD9	Tetraspanin super-family – EV-surface protein	Regulator of cell adhesion, marker of the Nerve growth factor (NGF)-secreting CD9+ Tendon stem cell population	(Fan et al., 2022)
CD11c	Integrin alpha-X	Receptor for fibrinogen	(Chiron et al., 2012)
CD14	Monocyte differentiation antigen	Co-receptor for bacterial lipopolysaccharide	(Daigneault et al., 2010)
CD19	B-lymphocyte antigen	Co-receptor for the B-cell antigen receptor complex (BCR)	(Stout et al., 2005)
CD20	B-lymphocyte antigen	Regulation of cellular calcium influx necessary for the development, differentiation, and activation of B cells	(Zhou et al., 2010)

CD24	Signal Transducer	Modulator of B-cell activation responses	(Lee et al., 2016)
CD25	Interleukin-2 receptor subunit alpha	Marker for immune cell activation	(Arvind et al., 2025)
CD29	Integrin beta-1	Extracellular matrix component	(Rieu et al., 2000; Shih et al., 2011)
CD31	Platelet endothelial cell adhesion molecule	Regulator of leukocyte trans endothelial migration (TEM)	(Graça et al., 2023)
CD40	Costimulatory surface molecule	Co-stimulator of T and B cells	(Rieu et al., 2000)
CD41b	Integrin alpha-IIb	Receptor for fibronectin, fibrinogen, plasminogen, prothrombin, thrombospondin and vitronectin	(L. Chen et al., 2014)
CD42a	Platelet glycoprotein 9	Mediator of platelet adhesion to blood vessels	(*High Throughput Assessment of Platelet Signaling, Function and Inhibition*, n.d.)
CD44	Cell-surface receptor	Regulator of activation, recirculation, and homing of T cells, CD44 might protect tendinopathic tendons from cellular senescence and decrease their disease activity by increasing tnmd expression	(S. Y. Chen et al., 2022), (Lui, 2015a)
CD45	Receptor-type tyrosine-protein phosphatase C	Positive regulator of T-cell coactivation	(Arvind et al., 2025)
CD49e	Integrin alpha-5	Receptor for fibronectin and fibrinogen, functional osteogenic capacity marker on MSCs	(Baksh et al., 2007)
	Neural Cell		

CD56	Adhesion Molecule 1	Cell adhesion molecules involved in neuron-neuron adhesion, neurite fasciculation, outgrowth of neurites	(Chua et al., 2014)
CD62P	P-selectin	Mediator of interaction between activated endothelial cells or platelets with leukocytes	(Kappelmayer & Nagy, 2017)
CD63	Tetraspanin super-family – EV-surface protein	Modulator of signal transduction, adaptor protein that links its interaction partners to the endocytic machinery of the cell	(Duffield et al., 2003)
CD69	Early activation antigen	Signal transmitting receptor in lymphocytes, natural killer cells, and platelets, activated T cells	(Garcia-Melchor et al., 2021)
CD81	Tetraspanin super-family – EV-surface protein	Modulator of signal transduction, expression associated with enhancd cellular uptake of extracellular vesicles	(Vogt et al., 2021),(Xue et al., 2022)
CD86	T-lymphocyte activation antigen	Co-stimulator of T cells proliferation and interleukin-2 production	(Tsuzaki et al., 2003)
CD105	Endoglin	Vascular endothelium glycoprotein that regulates angiogenesis, CD105-positive cells are associated with tenogenic potential	(Z. Chen et al., 2022)
CD133/1	Prominin-1	Regulator of cell differentiation, proliferation, and apoptosis, associated with tendon stem/progenitor cells (TSPCs)	(Tong et al., 2023), (Meregalli et al., 2010)
CD142	Tissue factor	Coagulation regulator, CD142+ MSCs functional MSC subtype, which promotes wound healing,	(H. Wang et al., 2025)
CD146	Melanoma Cell Adhesion Molecule	Cell adhesion molecule, tendon stem cells in the interfascicular matrix (IFM) express CD146, CD146+ cells are mobilised in response to tendon damage	(Marr et al., 2021)
CD209	C-type lectin receptor	Pathogen-recognition receptor	(Amraei et al., 2020; Li et al., 2022)
	Epithelial cell		

CD326	adhesion molecule	Cell adhesion regulator, amniotic epithelial cell marker	(Barboni et al., 2012, 2018)
HLA-ABC	Major Histocompatibility Complex class I	Immune response regulator	(Kragsnaes et al., 2014)
HLA-DRDPDQ	Major Histocompatibility Complex class II	Immune response regulator	(Russo et al., 2022)
MCSP	Melanoma-associated Chondroitin Sulfate Proteoglycan	Regulator of cell proliferation and migration, tendon stem cell marker	(Lui, 2015b)
ROR1	Neurotrophic Tyrosine Kinase, receptor-related 1	growth modulation in central nervous system tissues, romotes proliferation and skeletal muscle regeneration after injury.	(Kamizaki et al., 2017; Minami et al., 2010)
SSEA-4	Stage-Specific Embryonic Antigen-4	Marker of bone-marrow derived embryonic-like stem cells	(Pauly et al., 2010)

-

Supplementary Files

This is a list of supplementary files associated with this preprint. Click to download.

- FIGURESSUPPLEMENTARYINFO.xlsx